ENZYMATIC CROSSLINKING OF DYNAMIC HYDROGELS

FOR IN VITRO CELL CULTURE

A Thesis

Submitted to the Faculty

of

Purdue University

by

Matthew R. Arkenberg

In Partial Fulfillment of the

Requirements for the Degree

of

Master of Science in Biomedical Engineering

May 2018

Purdue University

Indianapolis, Indiana

THE PURDUE UNIVERSITY GRADUATE SCHOOL
STATEMENT OF COMMITTEE APPROVAL

Dr. Chien-Chi Lin, Chair

    Department of Biomedical Engineering

Dr. Hiroki Yokota

    Department of Biomedical Engineering

Dr. Dong Xie

    Department of Biomedical Engineering

Approved by:

    Dr. Julie Ji

        Head of the Graduate Program

ACKNOWLEDGMENTS

TABLE OF CONTENTS

LIST OF TABLES

LIST OF FIGURES

LIST OF ABBREVIATIONS

2D	2-dimensional
3D	3-dimensional
ECM	Extracellular matrix
4D	4-dimensional
SrtA	Sortase A
MT	Mushroom tyrosinase
PEG	Poly(ethylene glycol)
TGFβ	Transforming growth factor beta
LOX	Lysyl oxidase
PDAC	Pancreatic ductal adenocarcinoma
EMT	Epithelial-mesenchymal-transition
CSC	Cancer stem cells
Wnt	Wingless-related integration site
ROCK	Rho/Rho-associated kinase
MSC	Mesenchymal stem cells
iPSC	Induced pluripotent stem cells
pAA	Polyacrylamide
ISC	Intestinal stem cells
YAP	Yes-associated protein 1
UV	Ultraviolet
MeHA	Methacrylate-functionalized hyaluronic acid
DTT	Dithiothreitol
IR	Infrared radiation
PETMA	Pentaerythritol tetrakis(mercaptoacetate)

MMP	Matrix metalloprotease
HA	Hyaluronic acid
HRP	Horseradish peroxidase
DOPA	Dihydroxyphenylalanine
HPA	4-hydroxyphenyl acetate
NB	Norbornene
EGF	Epidermal growth factor
DCC	N,N-dicyclohexylcarbodiimide
DMAP	4-(dimethylamino)pyridine
HBTU	N,N,N,N-tetramethyl-O-($1H$-benzotriazol-1-yl)uronium hexafluorphosphate
HOBt	Hydroxybenzotriazole
IPTG	Isopropyl -D-1-thogalactopyranoside
DPBS	Dulbecco's Phosphate Buffered Saline
HBSS	Hank's Balanced Salt Solution
FBS	Fetal bovine serum
Anti-2	Antibioticantimycotic
DMEM	Dulbeccos modified eagle medium
ddH_2O	Double-distilled water
TFA	Trifluoroacetic acid
TIS	Trisisopropylsilane
LAP	Lithium phenyl-2,4,6-trimethylbenzoylphosphinate
OD_{600}	Optical density at 600 nm
cDNA	Complementary DNA
ANOVA	Analysis of variance
$SrtA_{7M}$	Heptamutant SrtA
$SrtA_{WT}$	Wild Type SrtA
SHH	Sonic hedgehog
ANKRD1	Ankyrin repeat domain 1

MDR1 Multi-drug resistance-1

MET   Mesenchymal-epithelial-transition

LIST OF NOMENCLATURE

G'   Storage modulus

G"   Loss modulus

$W_{dry,1}$ Dry weight 1

$W_{dry,2}$ Dry weight 2

Gel Fr   Gel fraction

$W_{swollen}$ Swollen weight

Q   Mass swelling ratio

W_0 Initial mass

W_t Final mass

ABSTRACT

Arkenberg, Matthew R. M.S., Purdue University, May 2018. Enzymatic Crosslinking of Dynamic Hydrogels for In Vitro Cell Culture. Major Professor: Chien-Chi Lin.

Stiffening and softening of extracellular matrix (ECM) are critical processes governing many aspects of biological processes. The most common practice used to investigate these processes is seeding cells on two-dimensional (2D) surfaces of varying stiffness. In recent years, cell-laden three-dimensional (3D) scaffolds with controllable properties are also increasingly used. However, current 2D and 3D culture platforms do not permit spatiotemporal controls over material properties that could influence tissue processes. To address this issue, four-dimensional (4D) hydrogels (i.e., 3D materials permitting time-dependent control of matrix properties) are proposed to recapitulate dynamic changes of ECM properties. The goal of this thesis was to exploit orthogonal enzymatic reactions for on-demand stiffening and/or softening of cell-laden hydrogels. The first objective was to establish cytocompatible hydrogels permitting enzymatic crosslinking and stiffening using enzymes with orthogonal reactivity. Sortase A (SrtA) and mushroom tyrosinase (MT) were used sequentially to achieve initial gelation and on-demand stiffening. In addition, hydrogels permitting reversible stiffening through SrtA-mediated peptide ligation were established. Specifically, poly(ethylene glycol) (PEG)-peptide hydrogels were fabricated with peptide linkers containing pendent SrtA substrates. The hydrogels were stiffened through incubation with SrtA, whereas gel softening was achieved subsequently via addition of SrtA and soluble glycine substrate. The second objective was to investigate the role of dynamic matrix stiffening on pancreatic cancer cell survival, spheroid formation, and drug responsiveness. The crosslinking of PEG-peptide hydrogels was dynamically tuned to evaluate the effect of matrix stiffness on cell viability and function.

Specifically, dynamic matrix stiffening inhibited cell proliferation and spheroid formation, while softening the cell-laden hydrogels led to significant increase in spheroid sizes. Matrix stiffness also altered the expression of chemoresistance markers and responsiveness of cancer cells to gemcitabine treatment. markers and responsiveness of cancer cells to gemcitabine treatment.

1. INTRODUCTION

1.1 Dynamic Biological Processes

ECM stiffening and softening are hallmarks of physiological and pathophysiological processes, including cancer progression, tissue fibrosis, and stem cell differentiation [1–3]. Specifically, variation of ECM mechanics could lead to changes in cell morphologies and behaviors [4, 5], differentiation potentials [6, 7], and protein secretion [8]. Matrix stiffening is caused by increased secretion of ECM (e.g., collagen) by stromal cells [9–11]. For example, primary human lung fibroblasts produce collagen in response to transforming growth factor beta (TGF-β) treatment [9]. In the lungs, TGF-β reduces matrix degradation, which leads to the formation of a dense, fibrotic tissue [9]. Enzymatic crosslinking can also increase matrix stiffness [12, 13]. For example, high expression of lysyl oxidase (LOX) leads to significant crosslinking between collagen and elastin molecules [12]. On the other hand, cell-mediated matrix degradation is enhanced via MMP secretion and activation [14]. MMPs target a wide range of ECM molecules, including proteoglycans, collagen, fibronectin, and laminin. This degradation leads to matrix softening.

1.1.1 Cancer Progression

Pancreatic ductal adenocarcinoma (PDAC) is a highly lethal cancer that has poor reception to chemotherapeutic agents [15, 16]. PDAC is characterized with a dense stroma [2] that promotes epithelial-mesenchymal-transition (EMT) and drug resistance [17]. While chemotherapy can effectively reduce the majority of tumor mass in a variety of cancers, cancer stem cells (CSCs) can survive leading to a generation of chemotherapeutically resistance cancer cells [18–20]. Matrix stiffening has been

reported to affect CSC growth and stem cell marker expression [21, 22]. For example, hepatic CSCs expressed higher level of stem cell markers, including CD133, EpCAM, Nanog, and SOX2. Furthermore, these cells had greater self-renewal and oxaliplatin resistance [22].

In addition to matrix stiffening, Shin and Mooney reported that matrix softening could alter mechanosensitivity of myeloid leukemia subtypes to drug actions [23]. Specifically, softening of the ECM enhanced cancer growth and led to increased resistance against cytosine arabinoside, a common leukemia treatment [23]. Kong and colleagues also demonstrated that matrix softening affects the phenotypes of hepato-carcinoma cells [8]. They reported that liver cancer cells underwent increased proliferation, downregulation of E-cadherin, and increased sensitivity to chemotherapeutic in the presence of protease-mediated, gradually softened collagen-based hydrogels.

1.1.2 Fibrosis

Fibrotic tissue is associated with significant deposition and crosslinking of fibrillar collagen by stromal cells. The generation of fibrotic tissue is further facilitated by LOX-mediated elastin and collagen crosslinking [3]. These phenomena lead to increased matrix stiffness and signaling events associated with inflammation. Matrix stiffening is both a hallmark of fibrosis and a significant contributer to its pathogenesis. Namely, increased matrix stiffening has been reported to enhance TGF-β response [24]. Additionally, ECM stiffening activates wingless-related integration site (Wnt) and interleukin signaling pathways [25, 26]. Tschumperlin and colleagues reported that matrix stiffening in fibrotic lung tissue inhibited synthesis of prostaglandin E(2), an inhibitor of fibrogenesis, indicating an important feedback relationship that enhances the development of fibrosis [27]. In a recent review, Lampi and Reinhart-King summarize the efficacy of targeting ECM stiffening and its cellular response [28]. They highlighted the necessity and challenges of targeting downstream signaling

pathways initiated by matrix stiffening (e.g., TGF-β and Rho/Rho-associated kinase (ROCK) intercellular signaling).

1.1.3 Stem Cell Differentiation

In addition to tumor progression and tissue fibrosis, Discher and colleagues reported that the mechanical properties of a stem cell niche play a significant role in directing the differentiation of mesenchymal stem cells (MSCs) into neurons, myocytes, and osteoblasts [29]. Culturing MSCs on collagen matrices with low (0.1-1kPa), medium (8-17 kPa), and high (25-40 kPa) stiffness led to phenotypic responses akin to neurogenic, myogenic, and osteogenic lineages, respectively [29]. Similarly, Prosper and colleagues demonstrated that seeding induced pluripotent stem cells (iPSCs) on fibronectin- or collagen-coated polyacrylamide (pAA) gels with different elastic moduli (i.e., 0.6, 14, and 50 kPa) lead to the expression of tissue specific markers [1]. However, it is important to note that these studies were performed on two-dimensional 2D substrates that do not fully recapitulate the 3D stem cell niche.

Many hydrogels have been designed to investigate the role of matrix stiffness on stem cell expansion and differentiation. For example, Lutolf and colleagues demonstrated the role of mechanically dynamic environments on differentiation and organoid formation of intestinal stem cells (ISCs) [6]. Specifically, stiff matrices containing fibronectin-derived peptide, RGD, were required for ISC expansion through yesassociated protein 1 (YAP) pathway. On the other hand, differentiation of ISCs into intestinal tissues required soft matrices and laminin-based adhesion. In addition, Shakesheff et al. reported that simultaneous alginate to collagen matrix switching and matrix softening decreased iPSC self-renewal and promoted differentiation into the three germ layers [30].

1.2   Engineering Strategies to Matrix Stiffening/Softening

Dynamic ECM-mimetic hydrogels with spatiotemporally tunable properties can facilitate research regarding cancer progression, fibrosis, stem cell fate, and many other biological processes. Generally, dynamic hydrogels permit time-dependent control of matrix properties (e.g., matrix stiffness). These hydrogels permit secondary crosslinking [31–34], site-specific degradation [35–38], or reversible crosslinking [39–42] upon exposure to an external stimulus (e.g., light, enzymes, or temperature) (Figure 1.1). Biomimetic hydrogels that afford temporal tunability of matrix properties are uniquely situated to elucidate many cellular processes. Synthetic approaches are particularly advantageous as simple, external stimuli can be exploited to permit user defined, on-demand matrix modification. However, stimuli such as Ultraviolet (UV)-light or heat may not be desirable. Additionally, these techniques could be improved to permit stiffening/softening with physiological timescales to mimic both short and long-term ECM modification.
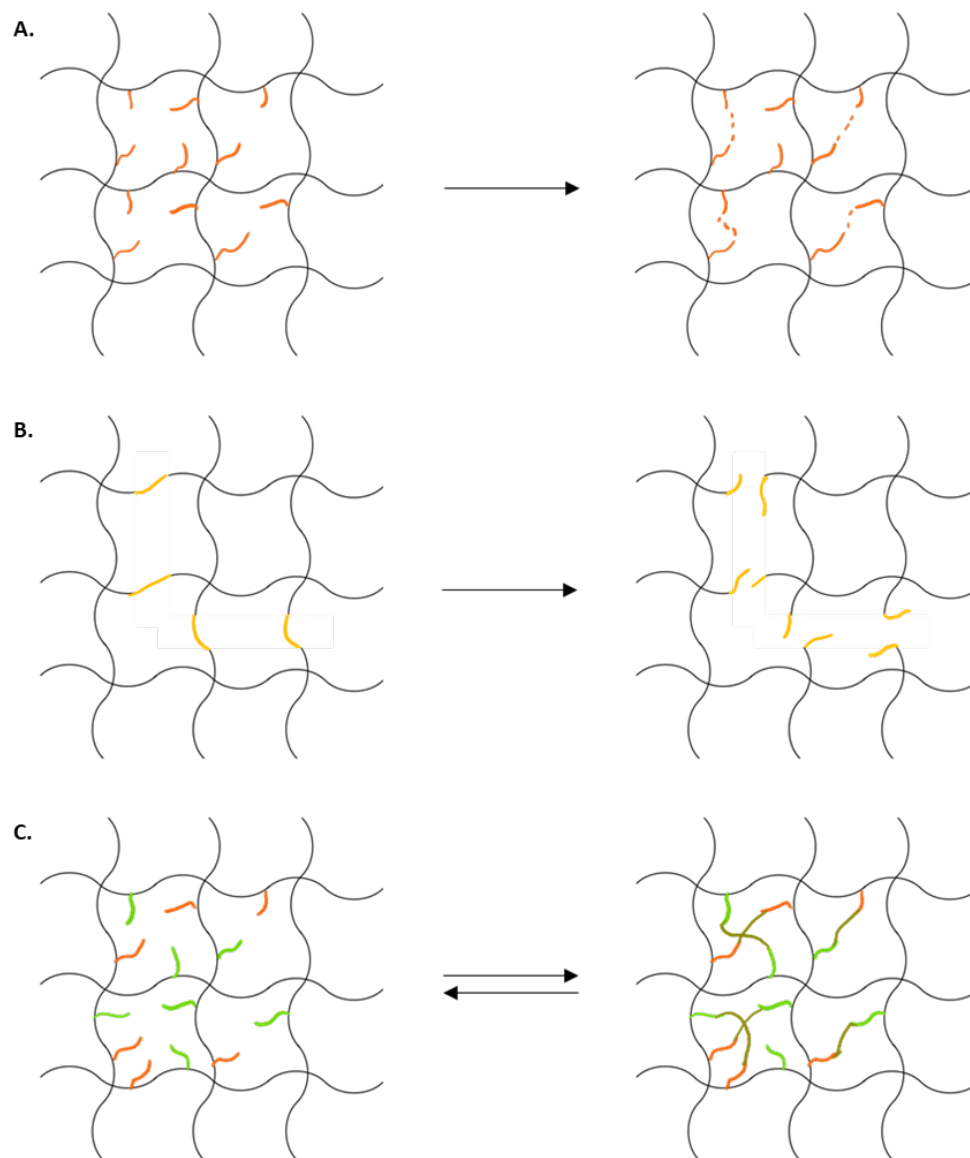
Fig. 1.1. Schematic representation of dynamic hydrogels (A) irreversibly stiffened, (B) irreversibly softened, and (C) reversibly stiffened.

1.2.1 Matrix Stiffening

Utilizing the secondary crosslinking concept, Burdick and colleagues designed methacrylate-functionalized hyaluronic acid (MeHA) hydrogels with tunable properties [31]. Hydrogels were initially crosslinked by methacrylated hyaluronic acid and

thiol-based crosslinker (e.g., dithiothreitol (DTT) with an off-stoichiometric ratio) via Michael-type addition. Light-and-radical-mediated chain growth polymerization of the remaining methacrylates was utilized to achieve matrix stiffening. In another example, Suggs et al. fabricated alginate hydrogels loaded with temperature-sensitive liposomes containing calcium ions and gold nanorods [32]. Upon infrared radiation (IR)-mediated heating of the gold nanorods, the liposomes were ruptured leading to release of calcium ions and further crosslinking of the alginate. Although this system afforded control of matrix stiffness spatiotemporally, the heat generated from IR irradiation may not be suitable for matrix stiffening. Gyarmati and Szilagyi reported that disulfide bond formation could be used to stiffen of hydrogels [33]. However, this approach may destabilize critical proteins and does not afford stringent control over the magnitude of stiffening.

1.2.2 Matrix Softening

Matrix softening typically occurs through hydrolytic [35, 36, 43] or enzymatic degradation [35, 38, 44]. For example, Metters and Hubbell reported the degradation kinetics of hydrogels containing hydrotically labile thioether-ester linkages [43]. A statistical-co-kinetic model was established to verify the hydrolytic degradation mechanism. Burdick and colleagues developed methacrylated hyaluronic acid hydrogels that contained both hydrolytically stable and degradable crosslinks [35]. Hydrolytically stable DTT and degradable pentaerythritol tetrakis(mercaptoacetate) (PETMA) were used to consume 20% and 65% of available methacryltes to permit partial degradation of hydrogels. Utilizing this system, it was demonstrated that stellate cells in a gradually softened environment (from 20 kPa to 3 kPa) reverted to myofibroblast phenotypes.

Cell-mediated enzymatic degradation can be achieved through the incorporation of protease-sensitive linkers such as matrix metalloprotease (MMP) or collagenase-sensitive linkers. West and Hubbell demonstrated this by fabricating a collagenase or

plasmin-sensitive copolymer through photopolymerization of acrylated PEG-peptide macromers. The APGL peptide and VRN peptides rendered the macromers labile to collagenase and plasmin, respectively [45]. Further, Chen et al. established a dextran methacrylate hydrogel crosslinked with MMP sensitive bis-cysteine containing peptides [46]. Permitting cell-mediated degradation led to single-cell migration and the strand-like invasion of endothelial cells typical of angiogenesis.

User-defined matrix softening can be achieved through the incorporation of photoresponsive linkers. For example, Anseth and colleagues utilized nitrobenzyl ether crosslinker to establish a photodegradable hydrogel permitting on-demand matrix softening [37]. Rapid (5 minutes) and stepwise degradation could be achieved through constant and pulsed UV exposure. This platform also permitted patterning of microscopic and macroscopic structures to study cell migration. In particular, local gel erosion led to increased spreading of fibrosarcoma cells.

1.2.3 Reversible Matrix Stiffening

In addition to matrix stiffening or softening alone, techniques to reversibly stiffen or soften hydrogels are increasingly being developed [39–42]. Anseth et al. utilized light-mediated azobenzene cis-trans isomerization to reversibly stiffen or soften hydrogels [39]. Moduli of the hydrogel was reversibly tuned ($\sim$100-200 Pa) upon UV or visible light exposure. In addition to the potential hazards of using UV light, a physiologically relevant degree of stiffening was not achieved. Anseth and colleagues later implemented a light-mediated reversibly stiffened hydrogel. Hydrogels were softened using the above mentioned nitrobenzyl photocleavage and stiffened using radical polymerization of methacrylate functional groups [40]. Alternatively, supramolecular host-guest interactions could be employed for reversible stiffening/softening hydrogels [41]. This was achieved by alternate addition and removal of macromolecular adamantane in cyclodextrin immobilized hydrogels. However, challenges to this approach include limited diffusion of macromolecular adamantane, as well as limited spatial

control of stiffening/softening. In another example, Cao et al. utilized Dronpa145N, a fluorescent protein to permit reversible stiffening [42]. Cyan and violet light exposure induced conformational switches between monomeric and tetrameric states of Dronpa145N, respectively. By fabricating protein polymers containing Dronpa145N either gel-sol (cyan) or sol-gel (violet) transitions could be achieved. However, the protein-polymer fabrication process was laborious, and 2 hours of illumination was required for the phase transition. Azobenzene and -cyclodextrin guest-host interactions have also been employed to fabricate reversibly stiffened HA-based hydrogels [47]. HA was modified with either azobenzene or -cyclodextrin to permit photoreversible interactions between each moiety. Upon 420 nm light exposure, guest-host interactions were formed due to azobenzene favoring a cis isomer state. This lead to an initially stiff matrix. Upon UV light (365 nm) exposure, a 60% reduction in modulus was attained owing to trans isomerization of azobenzene that led to decreased guest-host interactions. In addition, Wong and colleagues reports the use of an azobenzene photoswitchable crosslinker that confers matrix stiffening in the presence of blue light irradiation and matrix softening under UV light exposure [48]. MSCs seeded on stiffened substrates exhibited increased spreading with greater substrate stiffening. A potential challenge to this approach is the necessity for long term (1 hour) exposure to UV light.

1.3 Enzyme-mediated Crosslinking and Secondary Modifications of Matrix Properties

1.3.1 Enzymatic Crosslinking of Hydrogels

Biological reactions such as protein conformational changes and enzymatic reactions have been increasingly utilized to fabricate or to modify cell-laden hydrogels [49–53]. Table 1.1 summarizes current enzymatic techniques for hydrogel modification. For example, Lutolf et al. prepared hyaluronic acid (HA) based hydrogels utilizing transglutaminase-mediated HA-Glutamine and PEG-Lysine ligation [54]. Trans-

glutaminase catalyzes the isopeptide bond formation between the -amine of lysine and the -carboxamide of glutamine. However, transglutaminase has limited substrate specificity and calcium dependency. In another example, laccase, which catalyzes diphenol crosslinking, was utilized by Rocasalbas et al. to crosslink phenolic-conjugated gelatin and chitosan [55]. However, the hydrogels were formed in approximately two hours, rendering the system ineffectual for cell encapsulation. Martens and colleagues performed a comparative study of horseradish peroxidase (HRP), hematin, laccase, and tyrosinase to crosslink phenol-containing hydrogels [49]. HRP and hematin both require hydrogen peroxide and reduced cell viability immediately after encapsulation. On the other hand, laccase and tyrosinase resulted in higher cell viability and proliferation but took approximately 2.5 hours to fully crosslink. Furthermore, rotation of the samples was required to ensure a homogeneous distribution of cells. Phospho-pantetheinyl transferase, which catalyzes the reaction between the phosphopanethein prosthetic group of coenzyme A and a serine residue, was used by Lutolf and colleagues to crosslink PEG based hydrogels [56]. The reaction is highly specific, and the protein can be obtained in high expression yields. However, its magnesium-dependency is a notable drawback.

Table 1.1. Enzymatic crosslinking methods used for hydrogels.

Enzyme	Advantages	Disadvantages
Transglutaminase	• Efficient gelation • Cytocompatible crosslinking	• Short half-life • Limited substrate specificity
Laccase	• Simple phenolic substrates • Cytcompatible crosslinking	• Requires oxygen • Inefficient gelation
Horseradish Peroxidase	• Efficient gelation • Simple phenolic substrates	• Requires hydrogen peroxide
Tyrosinase	• Simple phenolic substrates • Cytocompatible crosslinking	• Requires oxygen • Inefficient gelation
Phosphopantetheinyl transferase	• High diffusivity (MW: 26 kDa) • Substrate specificity	• Requires coenzyme A and magnesium • Inefficient gelation
Sortase A	• High diffusivity (MW: 18 kDa) • Substrate specificity • Reversibility	• Hydrolytically degradable crosslinks

1.3.2 Enzyme-responsive Hydrogels

Enzyme-responsive polymers are being developed to confer matrix stiffening, softening, ligand removal, and ligand exchange. Ayyub and Kofinas utilized this concept to develop enzyme inducible stiffened nanoparticle-hydrogel composites [57]. Chymotrypsin-sensitive peptide, CY↓KC (arrow indicates enzyme cleavage site), and silica nanoparticles were incorporated into PEG-based hydrogels. Upon chymotrypsin-mediated cleavage of the peptide, adsorption and physical crosslinking the nanoparticles could occur leading to increased stiffening the hydrogels. Cell-mediated enzymatic removal of ligands has been demonstrated by conjugating bioactive moieties to

protease-sensitive pendent molecules [58,59]. This concept was demonstrated by Salinas and Anseth who designed a protease cleavable RGD tether [58]. In chondrogenic culturing conditions, MSCs secreted proteases that led to the cleavage and release of RGD. Thiol-acrylate hydrogels were fabricated with pendent MMP-13-sensitive RGD-containing peptides. Increased MMP-13 secretion was observed within 7 days of hMSC chondrogenesis, which led to cleavage and liberation of RGD motif. This led to enhanced chondrogenic phenotypes, as indicated by increased expression of type 2 collagen.

1.3.3 Mushroom Tyrosinase-mediated Dityrosine Formation

MT, also known as polyphenol oxidase, can be used to modify hydrogel properties owing to its catalytic activity in converting mono-phenolic residues into dihydroxyphenylalanine (DOPA) dimers [60] (Fig. 1.2).
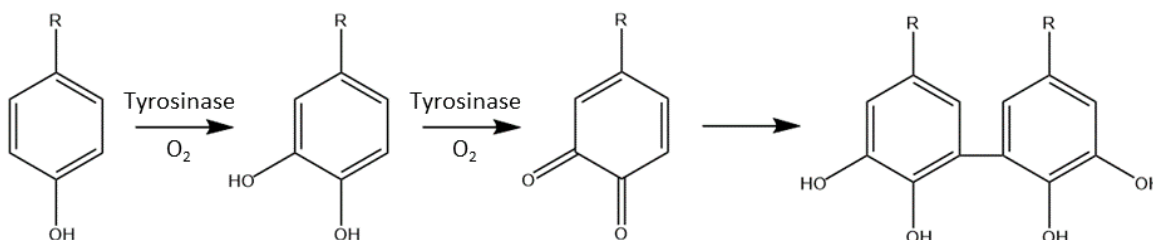
Fig. 1.2. MT-mediated dityrosine formation. MT catalyzes the oxidation of pendent tyrosine residues into dihydroxyphenylalanine (DOPA), DOPA quinone, and a DOPA dimer.

This enzymatic reaction has been used to irreversibly crosslink synthetic PEG-peptide hydrogels and natural gelatin-HA hydrogels. [34,61,62]. Using MT-triggered crosslinking, Liu et al. has recently demonstrated that hyaluronic acid and dynamic stiffening of gelatin-based hydrogels synergistically enhanced migratory phenotypes in PDAC cell types [62]. In particular, hydrogels consisting of thiolated-HA and

dually-functionalized gelatin (with 4-hydroxyphenyl acetate (HPA) and norbornene (NB) groups) were initially crosslinked through thiol-norbornene photoclick chemistry. Upon MT incubation, the HPA groups were dimerized, leading to higher matrix stiffness. In another example, MT was utilized to crosslink tyramine-conjugated hyaluronic acid and gelatin hydrogels [63]. The hydrogels exhibited tissue-adhesive properties, and the degradation kinetics were modulated by varying tyramine substitution and MT concentrations. While MT is useful in secondary crosslinking of hydrogels, its utility is limited by the available molecular oxygen, a co-factor for the reaction. Furthermore, MT-mediated reaction leads to irreversible increase in gel crosslinking, which precludes the use of this material system for studying the influence of matrix softening on cell behaviors.

1.3.4   Sortase A Peptide Ligation

Staphylococcus aureus SrtA is a low molecular weight ($\sim$18 kDa) transpeptidase with high substrate specificity [64]. Being a cysteine transpeptidase, SrtA covalently ligates two short peptide sequences, Leu-Pro-X-Thr-Gly (where X is any amino acid except proline) and an oligoglycine, G_n where n is greater than one (Fig. 1.3).
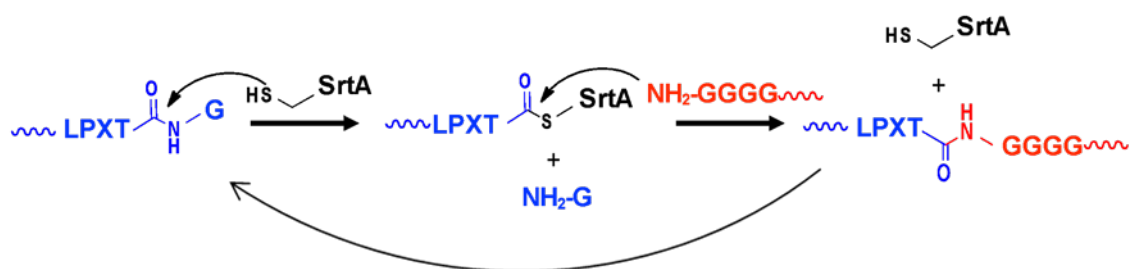
Fig. 1.3. Schematic of SrtA-mediated transpeptidation. Note that the final product, LPRTGGGG, can undergo further transpeptidation reactions.

Mechanistically, SrtA cleaves the amide bond between the Thr and Gly residues of LPXTG and forms a thioether intermediate that is resolved by a nucleophilic oligoglycine. Notably, this product is itself a substrate for future SrtA-mediated transpeptidation reactions, thus permitting reversible reactivity. SrtA has been used in a multitude of protein engineering applications including N- and C-terminal protein labeling [64], antibody modification [65, 66], and peptide cyclization [67]. Griffith and colleagues reported the first use of SrtA to perform primary crosslinking and modification of hydrogels [52, 68, 69]. PEG-peptide hydrogels were crosslinked using SrtA substrate functionalized PEG hydrogels. Additionally, epidermal growth factor (EGF) was modified with SrtA substrate NH_2-GGG (GGG-EGF). The growth factor was immobilized onto PEG hydrogels through incubation with SrtA. To remove the immobilized growth factor, SrtA with soluble glycine (GGG) was added.

1.3.5 Strategies to Immobilize Enzyme-responsive Substrates into Hydrogels

Biorthogonal reactions (i.e., cytocompatible chemistries with high selectivity and rapid kinetics [70]) are often employed to incorporate enzyme-sensitive substrates in hydrogel networks. For example, thiol-ene photoclick chemistry is widely utilized orthogonal chemistry in hydrogel fabrication and modification [71–74]. The mechanism by which thiol and ene moieties are crosslinked occurs under light exposure. Thiyl radicals, are generated by extraction of a hydrogen atom from the thiol group, form covalent bonds with an ene functional group to form a step growth network (Fig 1.4A). Due to the simplicity of enzyme substrates (e.g., GGG and LPXTG for SrtA and Y for MT), peptides can be designed and covalently immobilized to macromers using thiol-norbornene photoclick chemistry (Fig. 1.4B). This is advantageous due to its efficiency (∼30 min reaction time) and orthogonality between the cysteine-containing peptide and norbornene functionalized macromer. The peptide-

functionalized macromers can be subsequently crosslinked or modified using the above mentioned predictable and efficient enzymatic reactions.
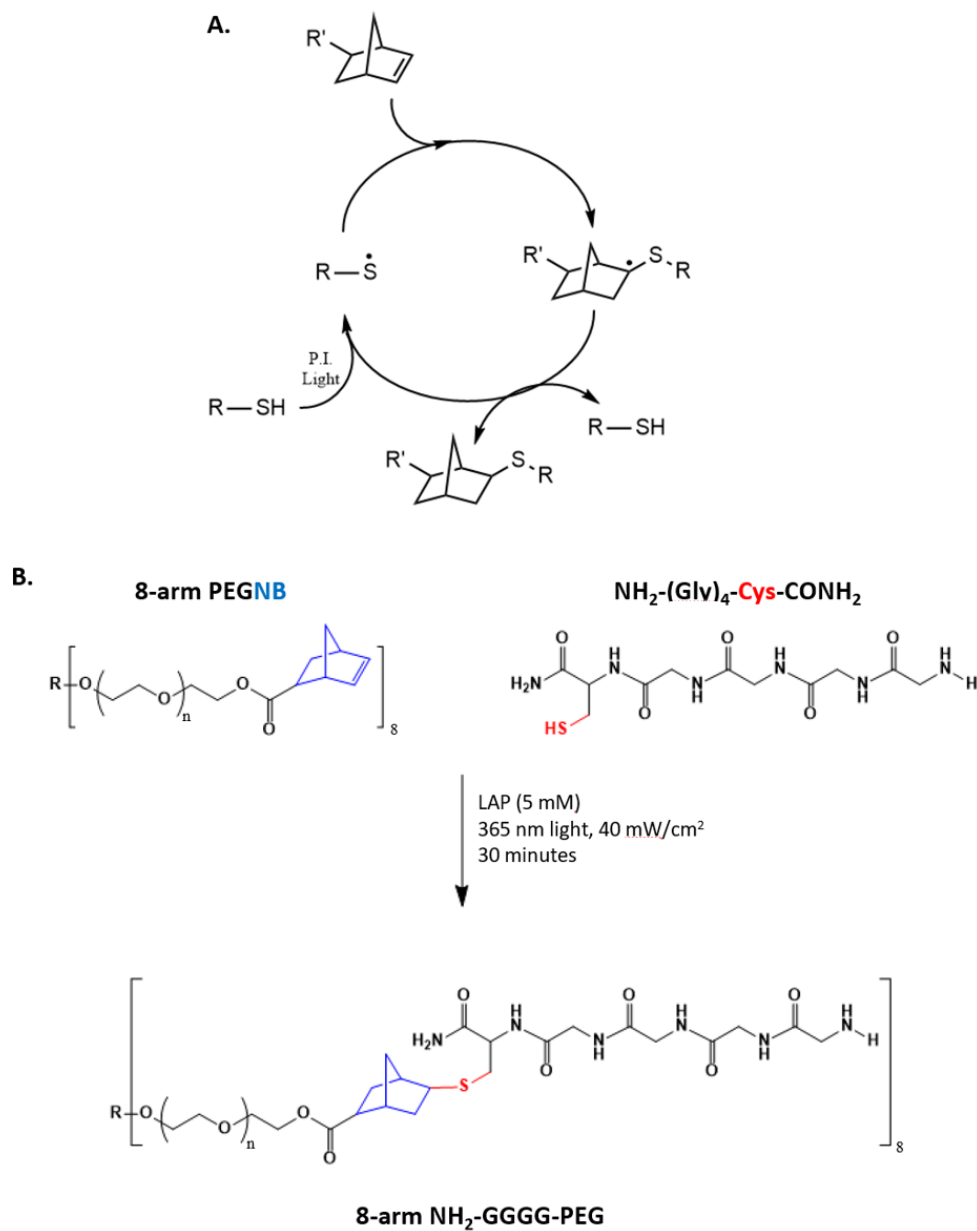
Fig. 1.4. Schematic representation of (A) thiol-ene step growth polymerization and (B) thiol-ene-mediated conjugation of pendent peptides to 8-arm PEGNB.

2. OBJECTIVES

2.1   Overview

Enzymatic reactions can overcome some of the challenges associated with synthetic approaches in crosslinking and modification of hydrogels. While SrtA peptide ligation has been used in hydrogel-based applications, the mechanical properties and gelation kinetics are not well characterized. In addition, its use in conjunction with additional enzymatic reactions such as MT-mediated dityrosine formation was not reported prior to this thesis work. Furthermore, the inherent reversibility of SrtA peptide ligation is advantageous for fabricating hydrogels with reversibly tunable properties. To demonstrate the utility of orthogonal enzymatic reactions to design hydrogels with temporally tunable properties, two objectives are proposed:

2.2   Objective 1: Establish Enzyme-mediated Reversible Crosslinking of Hydrogels

The first objective of this thesis was to use SrtA-mediated peptide ligation for crosslinking PEG-based hydrogels, followed by using MT-mediated dityrosine formation to tune matrix stiffness. By adjusting SrtA and substrate concentration, the rate of gelation and initial modulus was systematically altered. The enzymatic and hydrolytic degradation of SrtA-mediated crosslinked hydrogels in the presence of variable enzyme concentrations and soluble oligoglycine substrate were investigated. In addition, the cytocompatibility of SrtA-mediated crosslinking was established with MIN6, a mouse insulinoma cell line, and COLO-357 cells, a PDAC cell line. Matrix stiffening could be tuned by adjusting total tyrosine content and MT incubation time. In addition, the reversibility of SrtA-mediated transpeptidation was utilized to

fabricate hydrogels with reversible matrix stiffening. The degree of matrix stiffening was adjusted by varying SrtA concentration and incubation time, and softening was adjusted by varying enzyme as well as soluble glycine concentration. The process was also shown to be reversible for two cycles through alternate addition of Srt and SrtA with soluble glycine.

2.3 Objective 2: Investigate the Role of Matrix Stiffening on Cancer Cell Survival, Spheroid Formation, and Chemoresistance

After establishing a PEG-based hydrogel platform that permits tunable enzymatic crosslinking and on-demand stiffening/softening, the second objective was to evaluate the role of matrix stiffening on cancer cell survival and spheroid formation. Cell viability and spheroid diameter were monitored with and without MT-mediated hydrogel stiffening. The reversibility of SrtA peptide ligation was used to control spheroid formation of COLO-357 cells. Live/dead staining was used to determine cell viability and spheroid diameters. Lastly, COLO-357 cells in stiffened hydrogels were treated with gemcitabine to ascertain the effect of matrix stiffening on drug responsiveness in the cells. Metabolic activity and viability were monitored by AlamarBlue and live/dead staining, and cancer stem cell marker expression was analyzed by PCR. The results in this study establish the biological relevancy of our platform to investigate cancer cell survival in the presence of matrix stiffening.

3. MATERIALS AND METHODS

3.1 Materials

Eight-arm PEG-OH (20 kDa) was acquired from JenKem Technology, USA. 5-Norbornene-2-carboxylic acid, N,N-dicyclohexylcarbodiimide (DCC), 4-(dimethylamino)pyridine (DMAP), dimethyl phenylphosphonite, 2,4,6-trimethylbenzoyl chloride, 2-butanone, lithium bromide, and diethyl ether were obtained from Sigma-Aldrich. Fmoc-protected amino acids N,N,N,N-tetramethyl-O-(1H-benzotriazol-1-yl)uronium hexafluorphosphate (HBTU), and hydroxybenzotriazole (HOBt) were purchased from ChemPep or Anaspec. BL21 *E. Coli* was purchased from New England Biolabs. Kanamycin sulfate was obtained from IBI Scientific. Lysogeny broth, Lennox formulation, agar and broth were obtained from DOT Scientific. Isopropyl -D-1-thogalactopyranoside (IPTG) was obtained from Sigma Aldrich. Sensolyte© 520 Sortase A activity assay kit was obtained from Anaspec. Dulbeccos Phosphate Buffered Saline (DPBS), Hanks Balanced Salt Solution (HBSS), fetal bovine serum (FBS), 100X antibioticantimycotic (anti-2), and Dulbeccos modified eagle medium (DMEM) were purchased from Hyclone. Gemcitabine was obtained from TSZ CHEM. Mammalian cell Live/Dead staining kit was obtained from Life Technologies Corp. All other chemicals were obtained from Fisher Scientific unless otherwise noted.

3.2 PEG Macromer, Peptides, and Photoinitiator Syntheses

Eight-arm PEG-norbornene (PEG8NB, 20 kDa) was synthesized following previous protocols with minor modifications [75]. In anhydrous DCM, 5-norbornene-2-carboxylic acid (5-fold molar excess to hydroxyl groups on PEG, 5X) was reacted with DCC (2.5X) for 1 hour. The resulting norbornene anhydride was filtered to remove

by-product urea and added dropwise from an addition funnel to a two-necked round bottom flask containing 8-arm PEG-OH, DMAP (0.5X), and pyridine (0.5X) under nitrogen. The flask was covered and the reaction was allowed to proceed overnight. The process was repeated to improve norbornene functionalization of the PEG.The PEG8NB product was precipitated in cold diethyl ether and dried *in vacuo*. The dried product was redissolved in and dialyzed against double distilled H_2O (ddH_2O) for 3 days at room temperature (MWCO: 6000-8000 kDa), followed by lyophilization.^{1}H NMR (Bruker Advance 500) was used to confirm the degree of PEG functionalization (>90%, Appendix A).

All peptides (Table 3.1) were synthesized with standard Fmoc coupling chemistry in an automated, microwave-assisted peptide synthesizer (Liberty 1, CEM). The crude products were cleaved from resin in 95% trifluoroacetic acid (TFA), 2.5% ddH_2O, 2.5% Trisisopropylsilane (TIS), and 5% (w/v) phenol) for 3 hours at room temperature. The crude peptides were precipitated in cold ethyl ether and dried *in vacuo*. The dried peptides were purified using HPLC (Flexar system, Perkin Elmer) and confirmed by mass spectrometry (QTOF, Agilent Technologies). Ellmans assay (PIERCE) was used to quantify peptide stock concentrations by quantifying the concentration of the sulfhydryl group.

Table 3.1. Peptides used in enzymatic crosslinking of hydrogels.

Peptide	Primary Crosslinking Chemistry	Secondary Crosslinking Chemistry
NH2-GGGGC-CONH$_2$	SrtA-mediated peptide ligation	N/A
NH2-CYLPRTG-CONH$_2$	SrtA-mediated peptide ligation	MT-mediated dityrosine formation
NH2-GGG-CKGGGKC-LPRTG-CONH2	Thiol-ene photoclick chemistry	SrtA-mediated peptide ligation

Photoinitiator lithium phenyl-2,4,6-trimethylbenzoylphosphinate (LAP) was synthesized as described elsewhere [76]. Briefly, to a round bottom flask containing dimethylphenylphosphinate, an equal amount of 2,4,6-trimethylbenzoyl chloride was added under nitrogen. The reaction proceeded overnight. 4-molar excess of lithium bromide in 2-butanone was added to the reaction mixture that was heated to 50 ^{o}C. After 10 minutes, solid LAP was observed. The reaction mixture was cooled to room temperature and maintained for 4 hours. The mixture was filtered through a fritted funnel and washed with 2-butanone 3 times and cold ethyl ether to remove unreacted lithium bromide. ^{1}H NMR was used to confirm product formation.

3.3   PEG-peptide Conjugate Synthesis

PEG-peptide conjugates were prepared through thiol-norbornene photoclick chemistry by reacting purified cysteine-bearing peptides with PEG8NB. Peptide concentrations were determined through Ellmans assay. For conjugation to PEG8NB, desired amount of peptides (1.5-fold excess to norbornene groups) were added to a flask containing PEG8NB and photoinitator LAP (5 mM). The reaction mixture was exposed to light (Omnicure s1000, 365 nm, 40 mW/cm^2) for 30 minutes. To improve the conjugation efficiency, an additional 5 mM of LAP was added after 15 minutes. The products were dialyzed against ddH$_2$O for 2 days to remove excess peptides and LAP, followed by lyophilization to obtain purified PEG-peptide conjugates. The conjugates were stored at -20 ^{o}C prior to use.

3.4   Heptamutant Sortase A Expression and Purification

Calcium-independent, heptamutant SrtA (P94R, E105K, E108Q, D160N, D165A, K190E, K196T) was expressed as described elsewhere [77]. Competent BL21 *E. Coli* were transformed with pet30b-7M SrtA plasmid (a gift form Hidde Ploegh. Addgene plasmid # 51141) and grown on an LB-agar selection plate containing kanamycin (30 μg/mL). Individual colonies were picked and inoculated (220 rpm at 37 ^{o}C overnight

in 10 mL of LB media supplemented with kanamycin (30 μg/mL) The cultures were diluted 100-fold in LB media supplemented with kanamycin and shaken on an orbital shaker (220 rpm at 37 ^{o}C) until the optical density at 600 nm (OD$_{600}$) reached 0.4-0.6. SrtA expression was induced by adding IPTG (400 μM). Following 3 hours (220 rpm at 37 ^{o}C) of incubation, cells were isolated by centrifugation (8000 rpm, 15 minutes) and stored at -80 ^{o}C until lysis. Cell lysis was achieved by resuspending and incubating cells in lysis buffer (20 mM Tris, 50 mM NaCl, 0.2 mg/mL lysozyme, 1 mM PMSF, 1x Halt EDTA-free protease inhibitor Cocktail, and DNase I) for 30 minutes at 4 ^{o}C, followed by sonication 2 cycles of 3 minutes with 30% duty cycle, 20% amplitude followed by a 3-minute cool-down period). Lysates were cleared by centrifugation (10,000g, 20 minutes, 4 ^{o}C) and purified with His60 Ni Superflow resin and columns per manufacturers protocol. The purity of eluted fractions was analyzed by SDS-PAGE and Western blotting with anti-6X His tag antibody. Pure fractions were combined and concentrated to $\sim$60 mg/mL with Ultra-15 Centrifugal Filter Units (Amicon). Buffer exchanged was performed against DPBS with Zeba Spin desalting columns (MWCO: 7 kDa, Thermo Fisher Scientific). Concentrated SrtA aliquots were sterile filtered and stored at -80 ^{o}C prior to use. Stock concentrations were obtained by Ellmans assay by quantifying the free sufhydryl on SrtA. Heptamutant SrtA activity was verified against the wild type protein using Sensolyte© 520 Sortase A activity assay kit per the manufacturer's protocol.

3.5   Sortase A-mediated Hydrogel Crosslinking and Characterization

Hydrogels were fabricated by crosslinking PEG-YLPRTG and NH$_2$-GGGG-PEG with specified concentrations of SrtA as indicated. Both PEG-peptide macromers were dissolved in PBS and combined. For rheological analysis, SrtA was added to PEG-peptide mixtures and injected between two glass slides separated by 1 mm Teflon spacers. Gelation was performed for 10 minutes unless otherwise specified. Prior to rheometric measurement, hydrogels were incubated in PBS at 37 ^{o}C for 16

hours. Oscillatory rheometry in strain-sweep mode (CVO 100, Bohlin) was employed to measure the hydrogel storage and loss moduli (G' and G"). The reported storage modulus values were averaged from the linear region of the modulus-strain curves. In situ rheometry was performed in time sweep (0.5% strain, 1 Hz frequency, and 90 μm gap size at 25 ^{o}C) to obtain gelation kinetics. Immediately after adding SrtA, the precursor was injected between the rheometer platform and parallel plate geometry with the edge sealed with mineral oil to prevent evaporation.

To determine the swelling ratio and gel fraction, hydrogels were fabricated using the above-mentioned procedure and immediately dried *in vacuo*. After one day the dried hydrogel weight was measured and denoted as $W_{dry,1}$. The dried gels were then incubated in ddH$_2$O at 37 ^{o}C to remove sol fraction followed by a second 24 hour drying process to obtain dry weight two ($W_{dry,2}$). Gel fraction was calculated using the following equation:

$$Gel\ Fr.\ =\ W_{dry,2}/W_{dry,1}$$

To characterize swelling ratio, the hydrogels were swollen for 1 day in PBS at 37 ^{o}C and weighed to obtain the swollen weight ($W_{swollen}$). The mass swelling ratio (Q) was defined as:

$$Q\ =\ W_{swollen}/W_{dry,2}$$

3.6   Sortase A-mediated Hydrogel Degradation and Characterization

After SrtA-mediated polymerization of hydrogels, the initial mass (W_0) of the hydrogels was measured. The gels were then placed in wells containing varied concentrations of SrtA with soluble glycinamide (48 mM, 3-fold excess to crosslinker concentration) for transpeptidation-mediated degradation or SrtA only for SrtA-mediated hydrolytic degradation. Gels were removed from SrtA-containing solution at specified

time points, blotted dry, weighed (W_t), and returned to solution. This process was repeated until the gel was fully degraded. Results are presented as mass loss defined as:

$$Mass\ loss\ (\%)\ =\ 100*(W_t\text{-}W_0)/W_0$$

3.7   Sortase A-mediated Reversible Stiffening of Hydrogels

Hydrogels were fabricated using thiol-ene photopolymerization with macromer PEG8NB, peptide GGG-CKGGGGKC-LPRTG ($R_{thiol:ene} = 1$), and photoinitiator LAP (1 mM) by mixing components at desired concentrations and injecting the mixture between glass slides separated by 1 mm Teflon spacers as described above. The precursor solutions were subjected to 365 nm light (5 mW/cm^2, 2 minutes) for gel casting. To induce stiffening or softening, hydrogels were either incubated in buffer containing SrtA or SrtA with soluble glycinamide, respectively. Moduli were measured prior to and after stiffening or softening. Due to the volumetric shrinkage or swelling, the gap size was reduced from 750 μm to 500 μm for stiffening and increased from 500 μm to 650 μm for softening.

3.8   Mushroom Tyrosinase-mediated Stiffening and Characterization

Hydrogels were fabricated with the gelation method described in Section 3.5 and incubated for 16 hours prior to stiffening. To achieve stiffening, gels were placed in wells containing 1 kU/mL MT. Using oscillatory rheometry in strain-sweep mode as described above, moduli were measured prior to and after hydrogel incubation with MT (1 kU/mL) at 37 ^{o}C. Due to volumetric shrinkage of the stiffened gels, the gap size for $R_{GGGG:LPRTG} = 1$, $R_{GGGG:LPRTG} = 3$ were reduced from 525 μm to 475 μm and 700 μm to 625 μm, respectively.

3.9   MIN6 and COLO-357 Cell Culture

COLO-357 cells were maintained in high glucose DMEM containing 10% FBS and 1X-antibioticantimycotic (Anti-2). MIN6 cells, a mouse insulinoma cell line, were maintained in high glucose DMEM containing 10% FBS, and 1X-Anti-2 and 50 μM -mercaptoethanol. For both cell lines, media was refreshed every 2-3 days.

3.10   Sortase A-mediated encapsulation of MIN6, and Characterization of Cell Viability and Morphology

Prior to encapsulation, MIN6 and COLO-357 cells were trypsinized, counted (Countess© II Automated Cell Counter, ThermoFisher), and resuspended in HBSS or DPBS, respectively. The resuspended cells were mixed with sterile-filtered pre-polymer containing PEG-YLPRTG and NH_2-GGGG-PEG. SrtA was added to initiate gelation and the mixture was immediately injected into a 1 mL syringe mold. Curing proceeded for 10 minutes prior to placing the gels in fresh media. Metabolic activity was monitored with AlamarBlue reagent. In brief, COLO-357 and MIN6-laden hydrogels were incubated with AlamarBlue working reagent (diluted 10-fold with culture media) for 2.5 and 16 hours, respectively. Further, live/dead staining and imaging was implemented to assess cell viability per manufacturers protocols. Following washing to remove excess dye, stained cell-laden hydrogels were imaged by confocal microscopy (Olympus Fluoview FV100 laser scanning microscope). Z-stack images (100 μm thick with 10 μm slices) from one gel and at least three random fields were captured for each condition.

3.11   In situ Mushroom Tyrosinase-mediated stiffening of COLO-357-laden Hydrogels and Characterization of Cell Viability and Morphology

SrtA-mediated crosslinked cell-laden hydrogels were fabricated as described above. The hydrogels were transferred to a 24-well plate containing media supplemented with

1 kU/mL MT and incubated for 6 hours at 37 ^{o}C in 5% CO2 to induce stiffening. The hydrogels were transferred to and maintained in a new well containing fresh media. Live/dead staining and imaging was performed as described above and cell morphology was analyzed using Nikon NIS-element software.

3.12   Sortase A-mediated reversible stiffening of COLO-357-laden Hydrogels and Characterization of Cell Viability

Cells were encapsulated using the procedure described in Section 3.9 with modification. Photoinitator LAP was added to the precursor solution with cells. The mixture was injected into a syringe mold, and subjected to UV-light (365 nm, 5 mW/cm^2, and 2 min.). After casting, the gels were transferred to a 24-well plate containing fresh media. Cells were allowed to grow for 7 days prior to matrix stiffening by incubating the cell-laden hydrogels in media containing 50 μM of SrtA for 4 hours. On day 14, the hydrogels were subject to matrix softening through incubation in media containing 50 μM of SrtA and 15 mM glycinamide (3-fold to SrtA substrate concentration). Live/dead staining and imaging was implemented on day 1, 7, 14, and 21 to qualitatively investigate cell viability. Spheroid diameters were measured using Nikon NIS-element software.

3.13   Gemcitabine Resistance, Cell Viability, and Apoptosis Assays

Cells were encapsulated by thiol-ene photopolymerization using the methodology described in Section 3.12. After 3 days of growth, hydrogels were treated with SrtA (50 μM) for 4 hours to induce matrix stiffening. Four days post-stiffening the hydrogels were treated with 1 μM gemcitabine for 3 additional days. Metabolic activity and morphology of the cells were assessed by AlamarBlue reagent and Live/dead staining, respectively.

3.14   RNA Extraction and Real-time PCR

RNA isolation was completed using Nucleospin RNA isolation kit (Clontech). Briefly, 350 μL of lysis buffer was added to tubes containing cell-laden hydrogels. Subsequently, the hydrogels were homogenized using QIAShredder Homogenizer columns (Qiagen). Lysates were filtered, and RNA was precipitated through the addition of 70% ethanol and vigorous pipetting. Following desalting and wash steps, RNA was eluted with DNase/RNase-free H2O and quantified by spectrophotometry (Nanodrop 2000, Thermo Scientific).

Complementary DNA (cDNA) was generated by using Prime-Script RT reagent kit (Clontech) per the manufacturers protocol. Gene expression was analyzed by real time quantitative PCR using SYBR Premix Ex Taq II Kit (Clontech). All components (i.e., kit components, cDNA, and primers (Appendix B)) were mixed and transferred to a PCR plate. Analysis was completed using the 7500 Fast Real-Time PCR machine (Applied Biosystems), and results were analyzed using the $2^{-\Delta\Delta Ct}$ methodology. For all conditions, cycle count was standardized to GAPDH house-keeping gene (ΔCt) and normalized to the control group ($\Delta\Delta$Ct).

3.15   Statistics

Statistical analyses were conducted using either a two-tailed t-test or a two-way analysis of variance (ANOVA) and when permitted followed by a Bonferroni *post-hoc* test to evaluate significance between experimental groups. A p value < 0.05 was considered statistically significant. Single, double, and triple asterisks represent $p < 0.05, 0.01, 0.001$, respectively. All experiments were completed independently at least three times and quantitative results are presented as mean $\pm$ SEM.

4. RESULTS AND DISCUSSION

4.1 Validation of Heptamutant SrtA Enzymatic Activity and Calcium Independence

Heptamutant SrtA (i.e., $SrtA_{7M}$) was utilized throughout this thesis due to its improved stability and enhanced reactivity compared with the wild type SrtA ($SrtA_{WT}$) [78]. The mutations of P94R/D160N/D165A/K190E/K196T increase catalytic efficiency (k_{cat}/K_m) by 140-fold [79], whereas mutations E105K/E108A confer the reaction calcium-independent due to the stabilization of the critical calcium-binding $\beta6/\beta7$ loop [78]. The expression and purification of $SrtA_{7M}$ was confirmed by SDS-PAGE (Fig. 4.1A) and western blotting with antibody against hexahistadine tag (Fig. 4.1B).
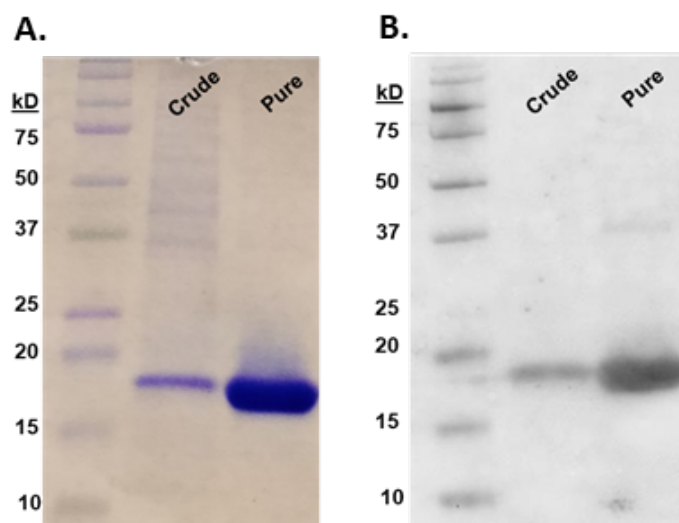
Fig. 4.1. (A) SDS-PAGE and (B) Western Blot of SrtA ($\sim$18 kDa) expressed in BL21 *E Coli.*

The catalytic activity of $SrtA_{7M}$ was verified by comparing against the commercially available $SrtA_{WT}$ in the absence or presence of Ca^{2+} (Figs. 4.2A and B, respectively). While both wildtype and heptamutant SrtA were active in buffer containing Ca^{2+}, only $SrtA_{7M}$ was active in a Ca^{2+}-deprived environment. Taken together, these results agree with the literature regarding the Ca^{2+}-independent enzymatic activity of $SrtA_{7M}$ [78, 80].
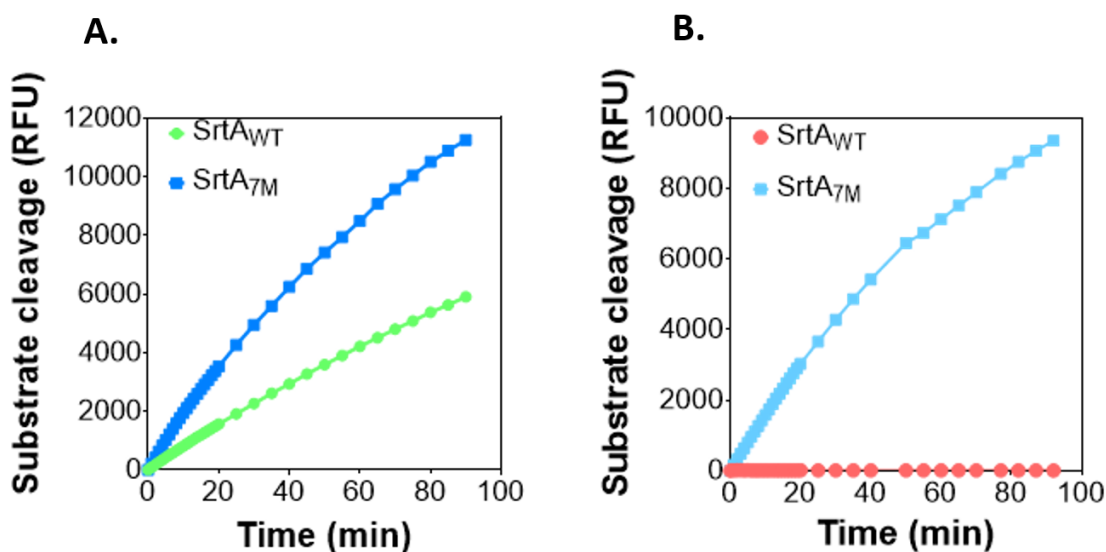
Fig. 4.2. Wild type SrtA ($SrtA_{WT}$) and Heptamutant SrtA ($SrtA_{7M}$) activity in Tris-HCl (pH=8.0) buffer with 50 nM SrtA, 2 μM 5-FAM/QXL FRET peptide substrate, and 2 mM oligo-glycine peptide (i.e., GGGGC) in the presence (A) or absence (B) of 10 mM $CaCl_2$. SrtA inducted substrate cleavage was detected by the fluorescence of the 5-FAM substrate (Ex/Em = 490/520). RFU: relative fluorescence units.

4.2 Gelation Kinetics of SrtA-mediated Crosslinking of PEG-peptide Hydrogels

To render hydrogels susceptible to SrtA-mediated crosslinking and MT-mediated secondary stiffening (Figs. 4.3 and 4.14), two sets of peptide substrates (i.e., CYLPRTG-

amide and NH$_2$-GGGGC-amide) were separately conjugated to PEG8NB macromers. Peptides bearing cysteine and tyrosine residues permit thiol-norbornene coupling of the PEG-peptide conjugates and MT-mediated stiffening, respectively (Fig. 1.5B).
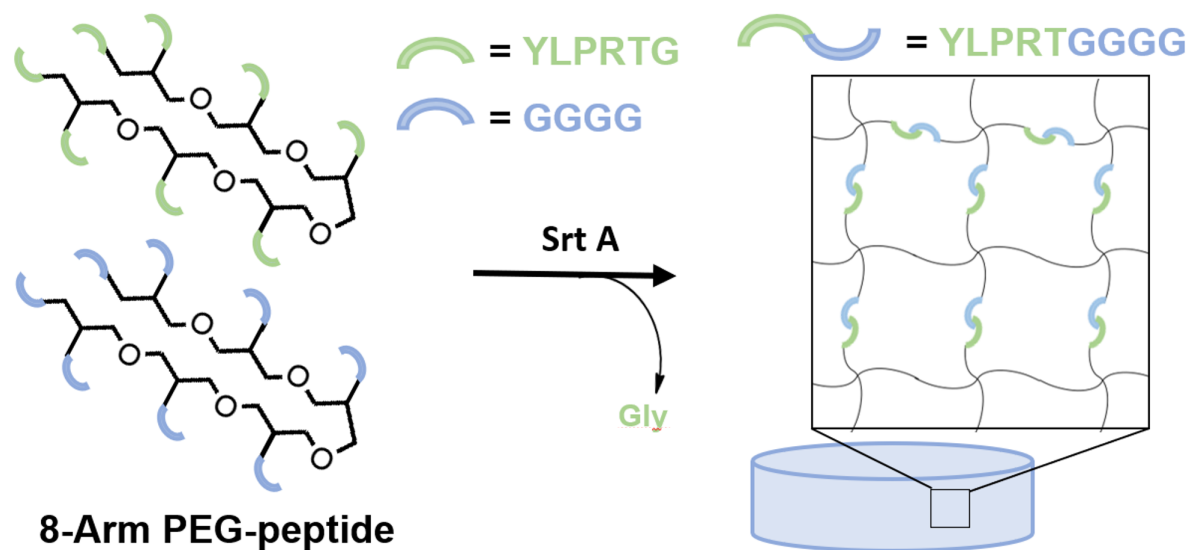
Fig. 4.3. Schematic of SrtA-mediated gelation. Peptides (YLPRTG and GGGG) were tethered to PEG macromers using thiol-norbornene click chemistry. Gelation was initiated after addition of SrtA.

Gelation kinetics at varied concentrations of SrtA (Fig. 4.3A) were determined by in situ rheometry. At a stochiometric equivalence of GGGG:LPRTG (R$_{GGGG:LPRTG}$ = 1) and a total PEG-peptide concentration of 2 wt%, higher concentrations of SrtA accelerated the speed of gelation as indicated by a rapid increase in shear modulus (G). Specifically, the gel point (the time in which the storage modulus crosses over the viscous modulus) for 150 μM, 300 μM, and 600 μM of SrtA were 302 s, 148 s, and 81 s, respectively). This was expected as higher enzyme concentrations increase the maximum velocity (V$_{max}$) of the transpeptidation reaction.
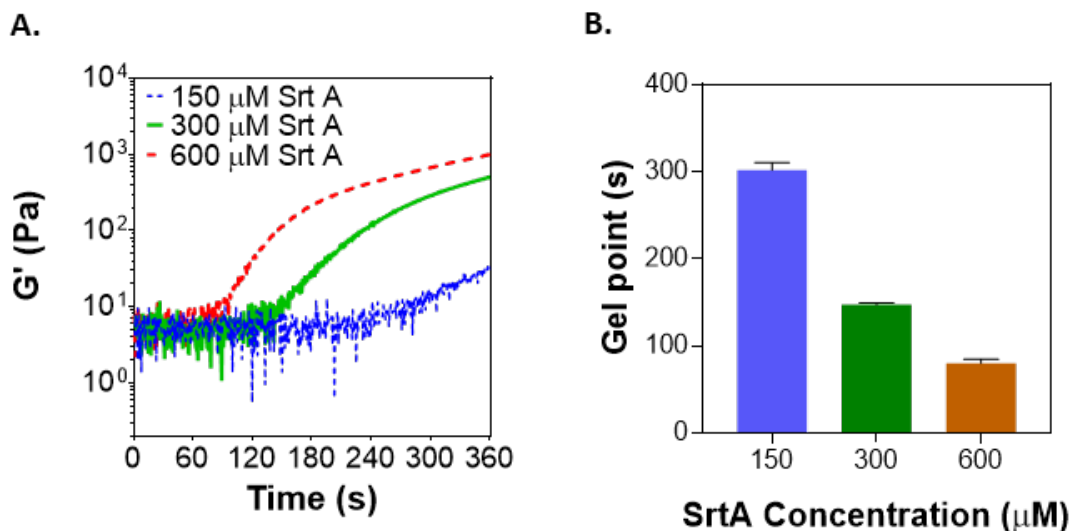
Fig. 4.4. (A) In situ rheometry of PEG-peptide (2 wt%, $R_{GGGG:LPRTG} = 1$) hydrogel crosslinking. G" omitted for clarity. (B) Gel points were calculated by determining the initial time point at which G′ was greater than G".

While gelation kinetics could be captured by in situ rheometry at higher concentrations of SrtA, a conventional tilt test can ascertain longer gelation times at lower enzyme concentrations (Fig. 4.5). Solutions of 6 wt% PEG-peptide ($R_{GGGG:LPRTG}=2$) were incubated at 25 ^{o}C with varied concentrations of SrtA. Like results shown in Figure 4.4, the gelation speed scaled with SrtA concentrations. Remarkably, the gelation time could be adjusted from a range of ∼10 minutes to ∼1.5 hours by simply adjusting the enzyme concentration without modifying other formulation parameters.
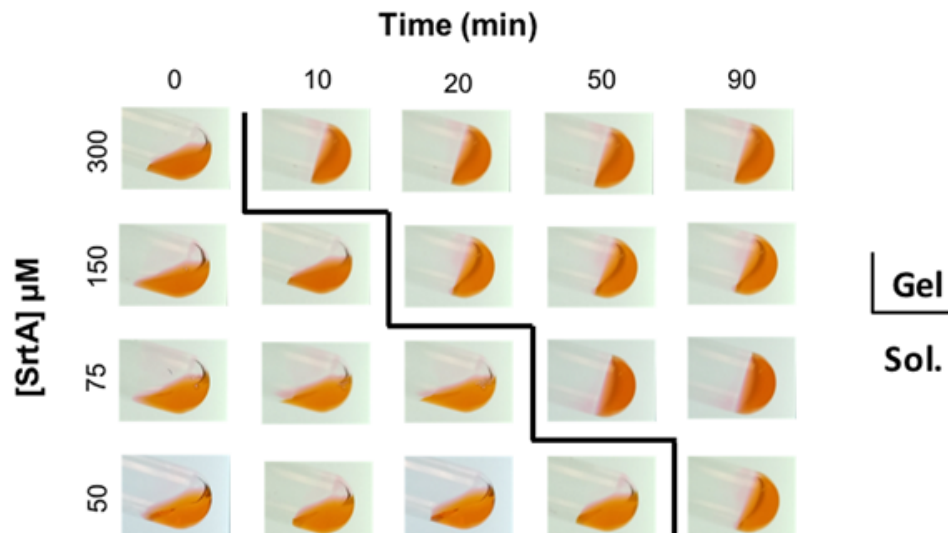
Fig. 4.5. Tilt test to track long-term gelation of PEG-peptide hydrogels. Eosin-Y (1 mM, red dye) was added for image clarity.

4.3 Effect of SrtA-mediated Crosslinking on the Modulus of PEG-peptide Hydrogels

Rheometry can be implemented to investigate the effect of SrtA concentration on the elastic modulus at a fixed total concentration of PEG-peptide (3 wt%, $R_{GGGG:LPRTG}$=1). The gelation continued at 37 ^{o}C for 10 minutes prior to placement in PBS buffer for equilibration (16 hrs.). At 10 minutes of gelation, concentration of SrtA did not significantly affect the final gel moduli (Fig. 4.6A). Furthermore, 300 μM of SrtA and 10 minutes of gelation was sufficient to complete gelation as extending the gelation time to 16 hours only moderately but not statistically significantly increased the gel moduli ($\sim$5,700, $\sim$6,350, $\sim$6,500 Pa for 10, 60, and 960 minutes of gelation, respectively. Fig. 4.6B). Moreover, tuning the total PEG-peptide concentration at a fixed $R_{GGGG:LPRTG}$=1 increased the moduli of hydrogels. Specifically, gel moduli were $\sim$2,700 Pa, $\sim$6,000, and $\sim$10,000 Pa for 2%, 3%, and 4% PEG macromer, respectively (Fig. 4.6C). These results suggested that it was possible to reach complete

gelation within 10 minutes using SrtA at as low as 150 μM. For the remainder of this study, 300 μM of SrtA was utilized for its gel point suitable for pipetting, solution mixing, and cell encapsulation. Together these results demonstrated exquisite control of matrix stiffness by adjusting gelation parameters such as enzyme concentration, gelation time, and total macromer concentration. Furthermore, the final crosslinking density of the hydrogels could be decoupled from gelation kinetics by simply varying the SrtA concentration.
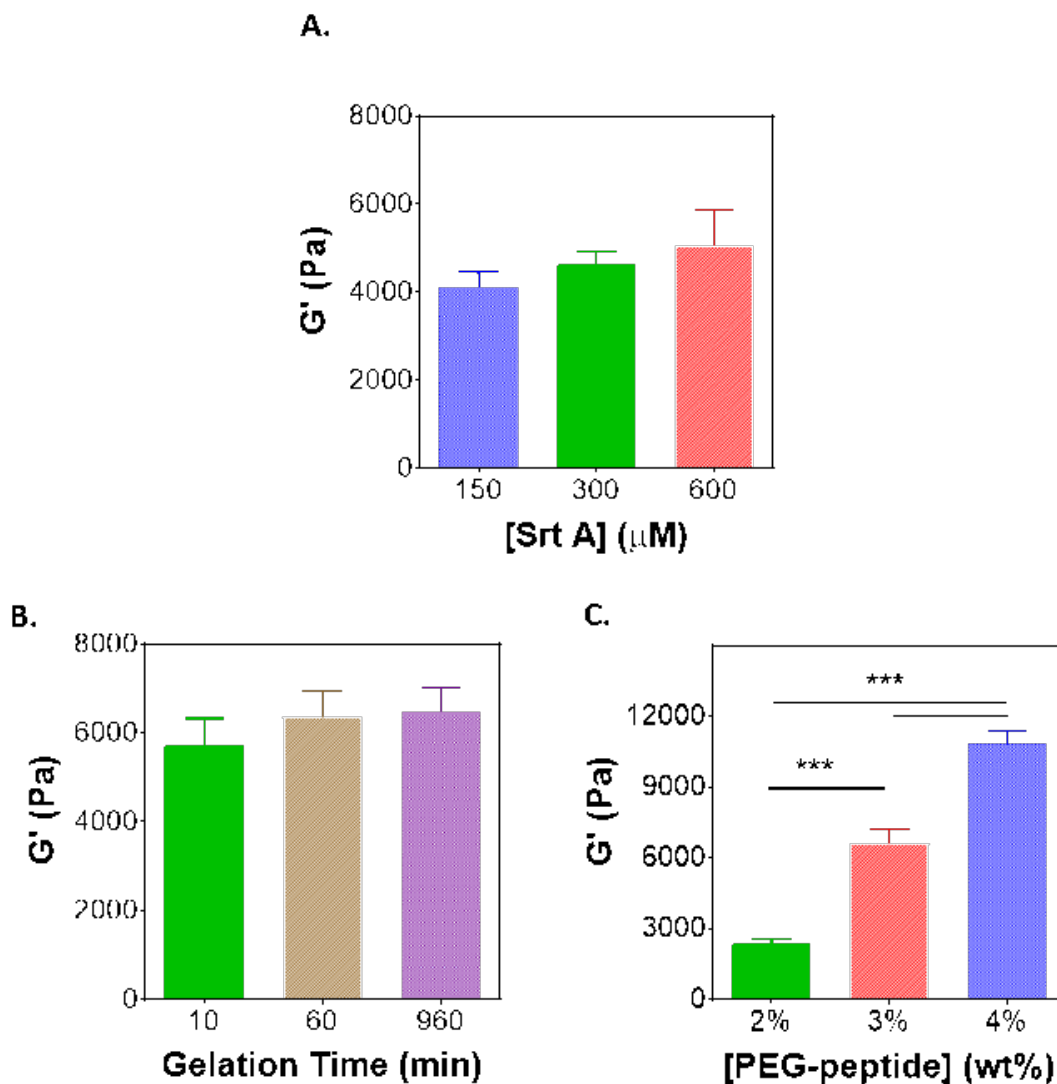
Fig. 4.6. (A) Effect of SrtA concentration on the modulus of PEG-peptide hydrogels (3 wt%, $R_{GGGG:LPRTG} = 1$). (B) Effect of gelation time on the modulus of PEG-peptide hydrogels (3 wt%, $R_{GGGG:LPRTG}=1$, 300 μM SrtA). (C) Effect of PEG-peptide concentration on the modulus of hydrogels (10 min gelation, 300 μM SrtA).

4.4 Effect of Substrate Ratio $R_{GGGG:LPRTG}$ on SrtA-mediated Hydrogel Crosslinking

The inherent reversibility of SrtA transpeptidation is a notable drawback of SrtA-mediated primary hydrogel crosslinking. This reversibility stems from the fact that cleaved glycine-containing by-products also serve as substrates for additional transpeptidation [81]. On the other hand, in solution with low glycine content, the thioacyl LPXT-SrtA intermediate can be hydrolyzed, rendering the product (i.e., LPXT-OH) unreactive for future transpeptidation reactions [81]. To investigate these phenomena and their effect on SrtA-mediated crosslinking, hydrogels were fabricated with different ratios of PEG-LPRTG and NH_2-GGGG-PEG substrates as per Table 4.1.

Table 4.1. Formulations of PEG-peptide hydrogels used in Figures 4.7 and 4.16.

$R_{GGGG:LPRTG}$	PEG-YLPRTG (wt%)	GGGG-PEG (wt%)	Total PEG (wt%)	[YLPRTG] (mM)	[GGGG] (mM)
1/3	1.5	0.5	2	6	2
1	1.5	1.5	3	6	6
3	1.5	4.5	6	6	18
3	2.5	7.5	10	10	30

The hydrogels containing an equimolar ratio of substrates exhibited higher moduli (G': ∼10,000 Pa) than the gels fabricated at $R_{GGGG:LPRTG}$=1/3 (G': ∼1000 Pa) and 3 (G: ∼1500 Pa Fig. 4.7A). This suggests that an equimolar ratio of substrate yielded a hydrogel network with less structural defects compared to hydrogels with off-ratio substrate concentrations. Hydrogels containing higher amounts of NH_2-GGGG-PEG substrate exhibited significantly higher gel fraction (0.4, 0.7, and 0.8 for $R_{GGGG:LPRTG}$ = 1/3, 1, and 3, respectively Fig. 4.7B). Hydrogels fabricated with $R_{GGGG:LPRTG}$ = 1/3 exhibited lower gel fraction potentially due to a loss of unreacted PEG-LPRTG.

We also speculate that an excess of unreacted NH_2-GGGG-PEG arms lead to network defects; however, the additional oligoglycine substrate drove the reaction towards transpeptidation, hence leading to increased gel fraction (Fig. 4.7B).
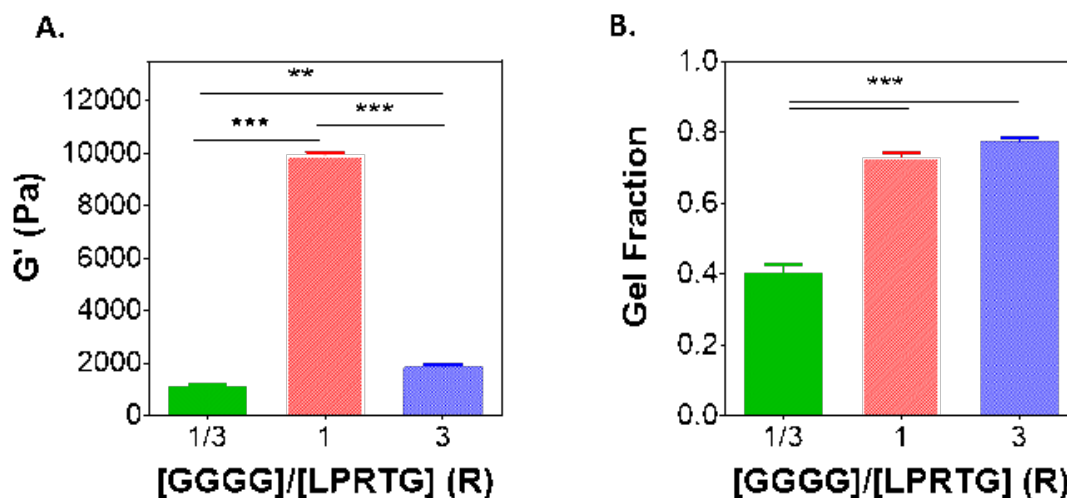
Fig. 4.7. (A) Effect of $R_{GGGG:LPRTG}$ on the hydrogel modulus. Gap sizes utilized for $R_{GGGG:LPRTG} = 1/3$, $R_{GGGG:LPRTG} = 1$, and $R_{GGGG:LPRTG} = 3$ were 475 μm, 525 μm, and 700 μm, respectively. (B) Effect of $R_{GGGG:LPRTG}$ on the gel fraction.

Notably, the effect of varying total PEG-peptide conc. at a fixed $R_{GGGG:LPRTG}$ = 3 had significant effect on the elastic modulus of the hydrogels. In particular, hydrogels fabricated at 6 wt% and 10 wt% of total PEG-peptide exhibited similar moduli ($\sim$1,000 Pa) while the modulus of 8 wt% hydrogels was significantly higher ($\sim$2,000 Pa, Fig. 4.8A). It was likely that at constant V_{max} for both conditions, additional time was necessary for SrtA to achieve complete gelation for the 10 wt% hydrogels. Further, at high concentrations, the macromer components may be functioning as crowding agents leading to enzyme aggregation and inactivity. This was observed through the formation of a white precipitate in the presence of increasing PEG-peptide concentration. This phenomenon further extends the time required for complete gelation.
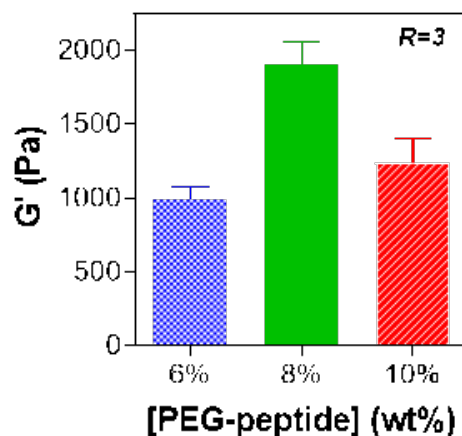
Fig. 4.8. Effect of total PEG-peptide concentration on modulus at $R_{GGGG:LPRTG} = 3$ (300 μM SrtA; 10 minute gelation time).

4.5   Degradability of SrtA-Crosslinked Hydrogels

The reversibility of the SrtA-induced transpeptidation can be utilized to erode PEG-peptide hydrogels. Specifically, incubating the hydrogels with additional SrtA and soluble glycine substrate leads to breakage of the LPRTG linker (i.e., transpeptidation mediated degradation. Fig. 4.9A). Even in the absence of glycine substrate, the LPRT-SrtA thiolether intermediate would gradually resolve, leading to hydrolytic cleavage of the peptide bond (Fig. 4.9B) and eventually hydrogel degradation. Both mechanisms can be used to control degradation of hydrogels (i.e., bulk degradation and surface erosion). Degradation can also be tuned without altering macromer and peptide concentrations. The degradation mechanisms were systemically studied due to their implications in drug delivery and tissue engineering applications.
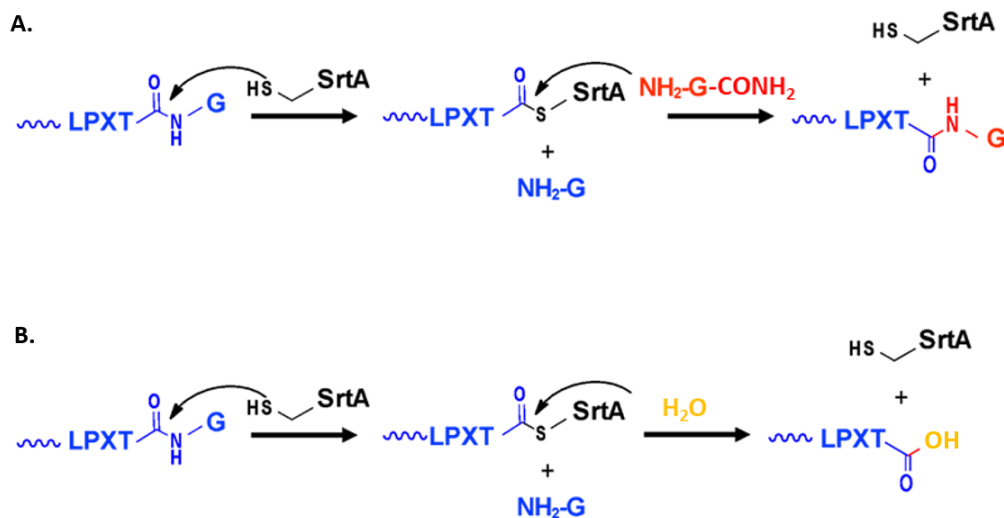
Fig. 4.9. Schematic of SrtA-mediated (A) transpeptidation and (B) hydrolytic degradation of PEG-peptide hydrogels.

To assess the effect of SrtA and a soluble, glycine-containing substrate on the transpeptidation-mediated degradation, hydrogels (6 wt%, $R_{GGGG:LPRTG}$=2) were fabricated as described above, washed extensively to remove residual SrtA, and incubated in buffer containing varying concentrations of SrtA and glycinamide (Fig. 4.10). As expected, degradation occurred in the presence of SrtA and glycinamide. This was evident by the initial swelling (i.e. negative loss of mass) of the hydrogel prior to the rapid decrease in mass. The enzyme treatment loosened the hydrogel network permitting initial water uptake and hydrogel swelling. For 10 μM, 25 μM, and 50 μM of SrtA, the gels reached complete degradation at approximately 9, 7, and 5 hours, respectively (Fig 4.10A). Further gels in the non-treated control group did not degrade. Additionally, the oliglycine concentration significantly affected the degradation rate. Hydrogels were treated with 50 M of SrtA and 16 mM and 48 mM of glycinamide (i.e., 1- and 3-fold to the glycine content in the hydrogels). As shown in Figure 4.10B, full degradation was achieved in 5 hours for a 3-fold concentration of soluble glycinamide. At a stochiometric ratio of soluble glycinamide to tethered

GGGG, the hydrogels degraded in 7 hours, suggesting higher concentrations of soluble substrate are required for faster degradation.
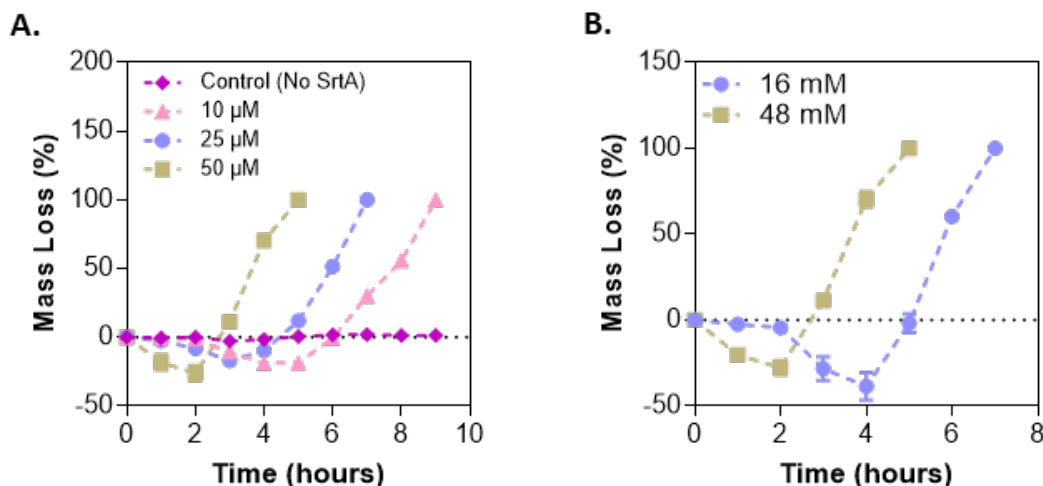
Fig. 4.10. Effect of (A) SrtA conc. and (B) NH_2-Gly-$CONH_2$ on SrtA mediated transpeptidation degradation of hydrogels (6 wt%, $R_{GGGG:LPRTG}=2$).

Compared with transpeptidation degradation, SrtA-mediated hydrolytic degradation (i.e., without soluble glycinamide as nucleophile) occurred much slower and appeared to proceed by way of surface erosion (Fig. 4.11). The gels degraded in $\sim$50 and $\sim$58 hours for 25 μM and 50 μM of SrtA, respectively. Similar to gelation kinetics, the degradation rates can be tuned in a range of hours up to multiple days. Further, the degradation rate can be slowed or stopped by washing the hydrogels to remove SrtA. This can be exploited in the future for investigating cell behaviors in a gradually degrading microenvironment. As opposed to other protease (e.g., MMPs) degradation mechanisms, SrtA transpeptidation is highly specific and does not interfere with cell-mediated protease activity. In addition, the selectivity of SrtA transpeptidation allows for degradation without affecting large ECM proteins (e.g., collagen). These proteins can be later assayed for functional characterization of cell response and protein secretion.
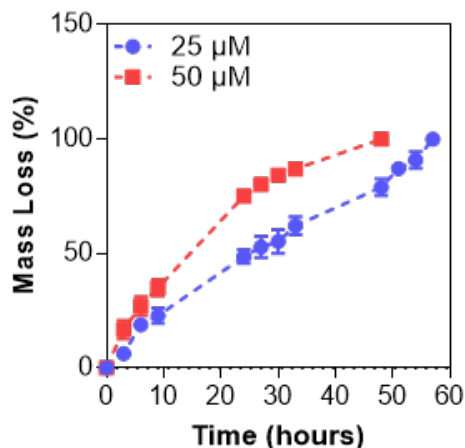
Fig. 4.11. Effect of SrtA concentration on SrtA-mediated hydrolytic degradation of PEG-peptide hydrogels (6 wt%, $R_{GGGG:LPRTG} = 2$).

4.6 Cytocompatibility of SrtA-crosslinked Hydrogels

In situ encapsulation of mouse insulinoma cell line MIN6 and pancreatic cancer cell line COLO-357 were utilized to demonstrate the cytocompatibility of the SrtA-mediated gel crosslinking (Figs. 4.12 and 4.13). COLO-357 was used as a model cell line for spheroid formation in the presence of dynamic stiffening, whereas MIN6 beta-cells were encapsulated due to their vulnerability in bio-inert hydrogels at a relatively low cell density [72,82]. From a previous report, it was suggested that approximately 0.3% of mammalian cell proteins contain the LPXTG substrate [69]. Therefore, SrtA-mediated transpeptidation would have superior biocompatibility. Similar to reported results [83], live/dead stained images showed that virtually all cells remained alive following encapsulation (day 1). Furthermore, the encapsulated cells formed spheroids by day 10 of in vitro culture in 3 wt% hydrogels ($R_{GGGG:LPRTG}$=1) (Fig. 4.12A). The encapsulated MIN6 cells exhibited increasing metabolic activity over the course of 7 days, suggesting the cells maintained their ability to proliferate even in the bio-inert hydrogels (Fig. 12B).
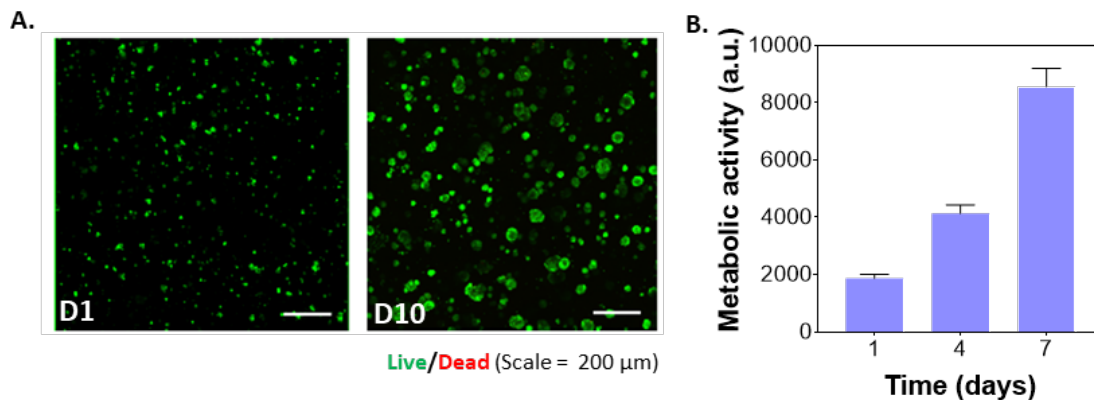
Fig. 4.12. Effect of SrtA-mediated crosslinking on the viability and metabolic activity of MIN6 cells. (A) Representative z-stack images of live/dead stained cells (2×10^6 cells/mL) encapsulated in PEG-peptide hydrogels, 3 wt%, $R_{GGGG:LPRTG} = 1$). (B) The metabolic activity of encapsulated MIN6 cells (n = 3).

Similar to the encapsulation of MIN6 cells, nearly all COLO-357 cells remained alive after encapsulation (day 1). The cells were metabolically active and formed spheroids by day 7 (Fig. 4.13). There results were consistent with previous report for this cell type cultured in 3D where metabolic activity peaked at around day 4, followed by a steady decrease for the next 3 to 5 days [84]. The results here demonstrated the cytocompatibility of SrtA-mediated crosslinking owing to the high substrate specificity of the transpeptidation reaction. Although this thesis only explored the encapsulation of COLO-357 and MIN6 cells, SrtA could potentially be used to encapsulate a variety of mammalian cells, including stem cells.
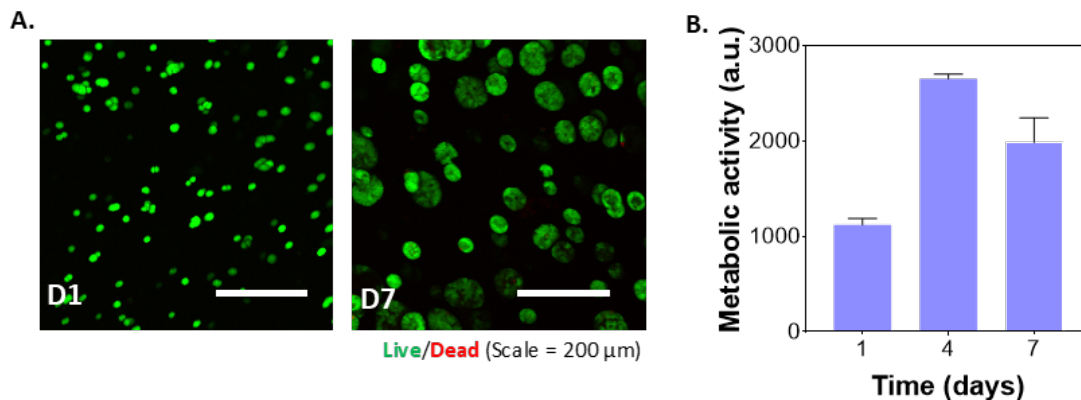
Fig. 4.13. Effect of SrtA-mediated crosslinking on the viability and metabolic activity of COLO-357 cells. (A) Representative z-stack images of live/dead stained cells (2×10^6 cells/mL) encapsulated in PEG-peptide hydrogels, 3 wt%, $R_{GGGG:LPRTG} = 1$). (B) The metabolic activity of encapsulated MIN6 cells (n = 3).

4.7   Mushroom Tyrosinase Stiffening of SrtA-crosslinked Hydrogels

As described by Liu et al., MT-stiffening is advantageous due to the simplicity of the tyrosine substrates and the predictable reaction kinetics [34, 62]. To permit MT-mediated stiffening in SrtA-crosslinked hydrogels, a single tyrosine residue was incorporated in the PEG-peptide conjugate (i.e., PEG-Y-LPRTG). MT incubation led to increased crosslinking density and matrix stiffness through dityrosine formation (Fig. 4.14).
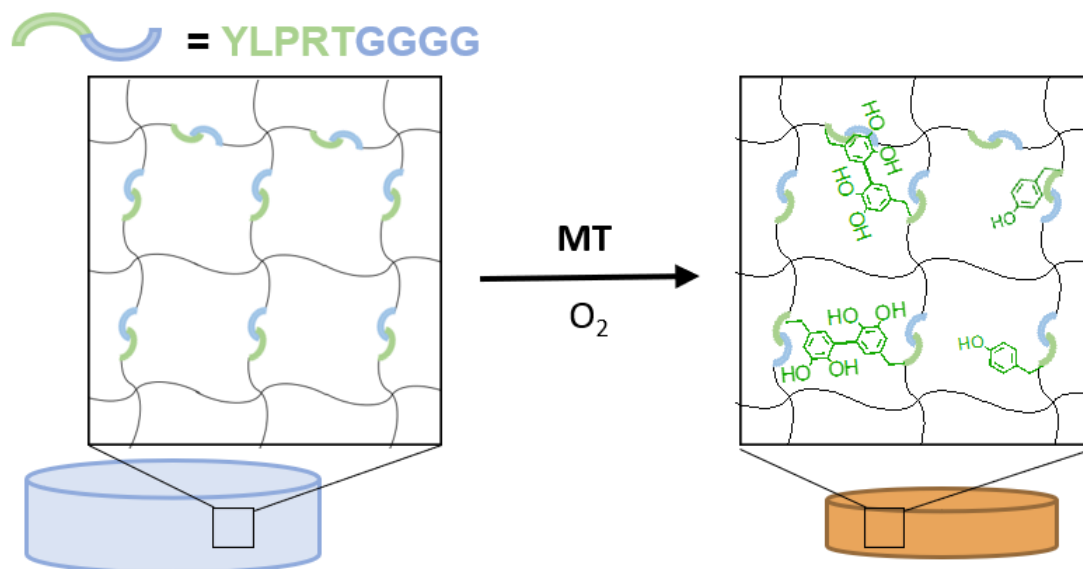
Fig. 4.14. Schematic of MT-mediated dityrosine formation. Secondary crosslinking
was achieved upon incubation with MT.

After equilibration, the gels were placed in buffer containing MT (1 kU/mL).
For 3 and 6 hours of MT incubation, the moduli of hydrogels increased ∼1.25-fold
and ∼1.5-fold, respectively (Fig. 4.15A). In addition, dityrosine formation caused
yellowing/browning of the hydrogels, which was accompanied by volumetric shrinkage
of the gels. After 6 hours of MT incubation, the hydrogels underwent a 25% reduction
in size (Fig. 4.15B). These results indicated that on-demand matrix stiffening could
be achieved by simply incorporating tyrosine residues into the peptide linker of SrtA-
mediated crosslinked hydrogels. Additionally, the stiffening could be tuned by simply
adjusting MT incubation time.
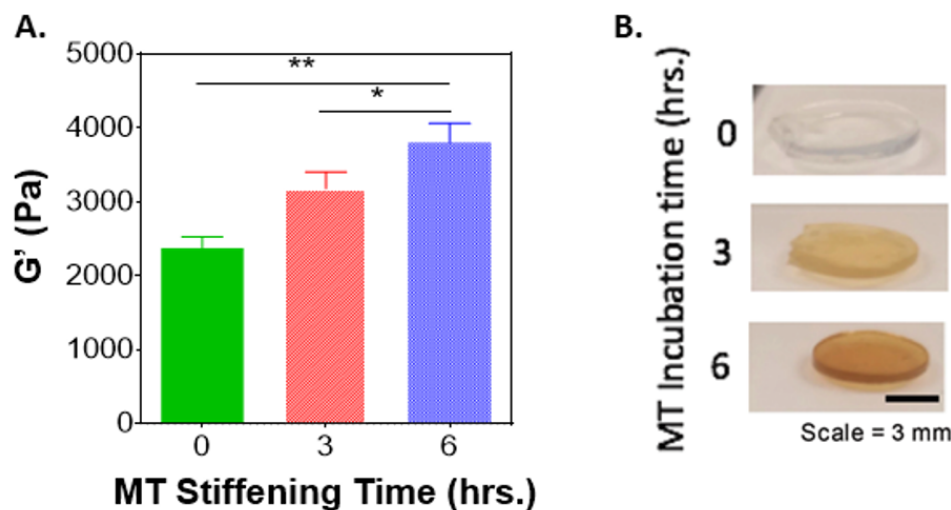
Fig. 4.15. (A) Effect of MT incubation time on the modulus of PEG-peptide hydrogels (2 wt%, $R_{GGGG:LPRTG} = 1$, MT = 1 kU/mL). (B) Representative images of hydrogels incubated with MT for varying durations.

As demonstrated in Figures 4.7 and 4.8, substrate ratio plays a significant role in determining the properties of SrtA-mediated crosslinked hydrogels. Hydrogels were fabricated per table 4.1. For the 6 wt% and 10 wt% hydrogels, a fixed ratio of 3 was used due to its desirable gel properties (low modulus and high gel fraction). While both conditions exhibited similar initial shear moduli of ~1 kPa, MT incubation yielded higher moduli ~3 kPa) in 10 wt% gels compared to 2 kPa for 6 wt% (Fig. 4.16). The higher degree of stiffening for 10 wt% hydrogels can be attributed to a higher concentration of tyrosine residues (Table 4.1).
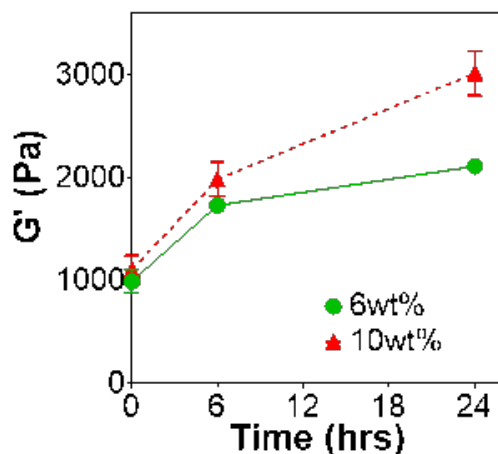
Fig. 4.16. MT-mediated stiffening of PEG-peptide hydrogels ($R_{GGGG:LPRTG} = 3$, MT = 1 kU/mL).

4.8 Effect of MT Stiffening on the Generation of COLO-357 Spheroids

It is known that matrix stiffness plays a significant role on pancreatic cancer cell growth and morphology [84]. High crosslinking density of cell-laden hydrogel could cause significant strain on cells and inhibit their proliferation, whereas low crosslinking density allows for hydrogel deformation by proliferating cell spheroids. Nonetheless, the effect temporal changes in hydrogel crosslinking density on cell behaviors remains challenging technologically.

To study the effect of dynamic matrix stiffening on COLO-357 spheroid morphology, PEG-peptide hydrogels (10 wt%, $R_{GGGG:LPRTG} = 3$) were fabricated for their desirable initial modulus, gel fraction, and magnitude of stiffening (Figs. 4.7 and 4.16). It is important to note that the hydrogels were crosslinked without protease sensitive linkers to study the sole effect of matrix stiffening without complication of cell-mediated gel degradation. As shown in Figure 4.17, matrix stiffening inhibited proliferation of COLO-357 cells, as indicated by the formation of cell spheroids with smaller diameter. These results are consistent with previous reports on the effect of

static matrix stiffness on COLO-357 spheroid sizes [84]. Both SrtA-mediated primary and MT-mediated secondary crosslinking mechanisms did not induce cell damage as no dead cells were observed in the live/dead staining images. While matrix stiffening process was performed for 6 hours in this thesis work, it could be extended to multiple days using lower enzyme concentration or by performing a step-wise stiffening procedure (i.e., incubate gels with MT in short periods of time periodically) to mimic the timeframe of in vivo matrix stiffening.
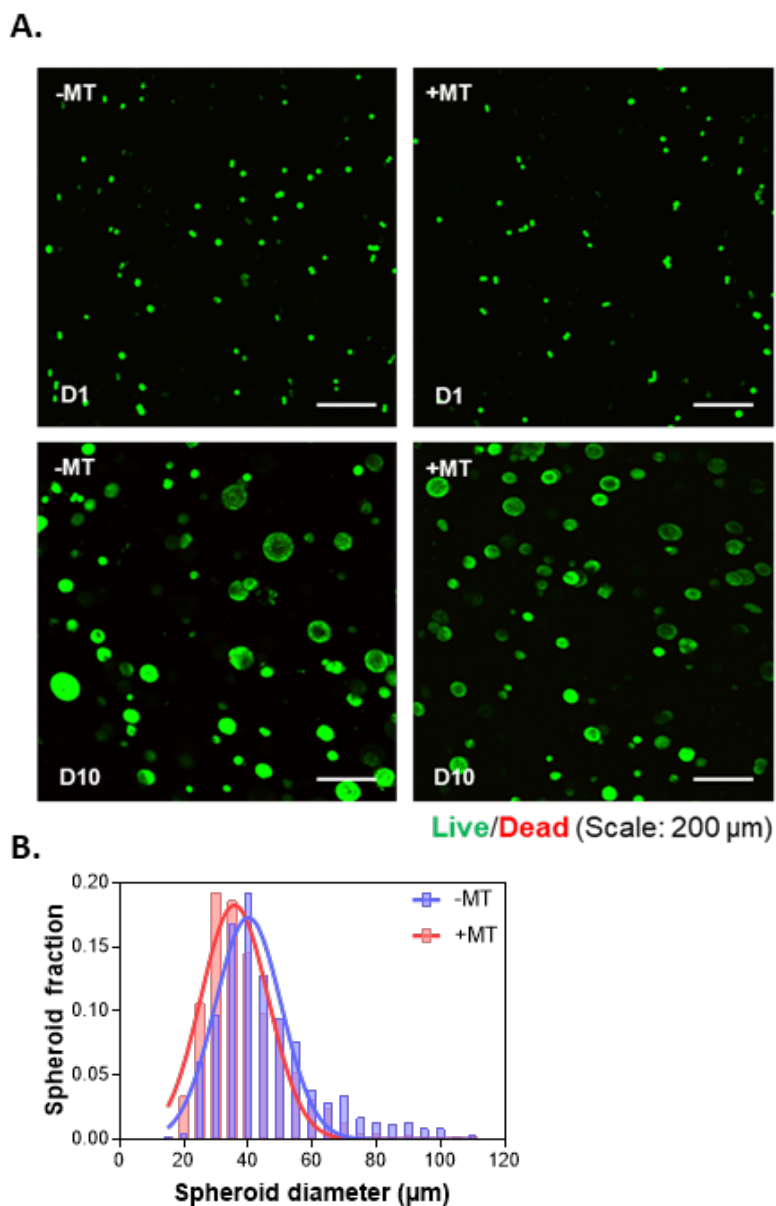
Fig. 4.17. (A) D1 and D10 live/dead images of COLO-357 cells (2×10^6 cells/mL) with or without MT incubation (D1 stiffening, MT incubation time = 6 hrs.). (B) Cell spheroid distribution with or without MT-mediated stiffening. Diameters were quantified day 10 post-encapsulation. The diameters of the spheroids with and without MT stiffening were 45.91 ± 0.67 μm (n = 594) and 39.48 ± 0.51 μm (n = 590), respectively. A two-tailed t-test was performed for statistical analysis (p < 0.01).

4.9   SrtA-mediated Reversible Stiffening

In addition to degradation of PEG-peptide hydrogels, SrtA-mediated transpepti-dation is a suitable approach for reversible matrix stiffening, and this approach has not been reported in the literature. To prepare hydrogels with reversible stiffen-ing/softening capability, hydrogel was first prepared by thiol-norbornene photoclick chemistry with PEG8NB as a macromer and a unique linear peptide bearing bis-cysteine residues and pendent SrtA substrates (i.e., GGG-CKGGGKC-LPRTG). This approach is advantageous due to the orthogonality of the thiol and norbornene func-tional groups and the quantitative immobilization of the SrtA peptide substrates (Fig. 4.18). Through SrtA-mediated transpeptidation, the pendent peptides are covalently ligated resulting in increased crosslinking density and matrix stiffness. When needed, the stiff hydrogel can be softened through incubation with SrtA and an excess of soluble glycine substrate. In theory, this process could be repeatedly indefinitely if SrtA-mediated hydrolytic degradation of the peptide bond is minimized by extensive washing.
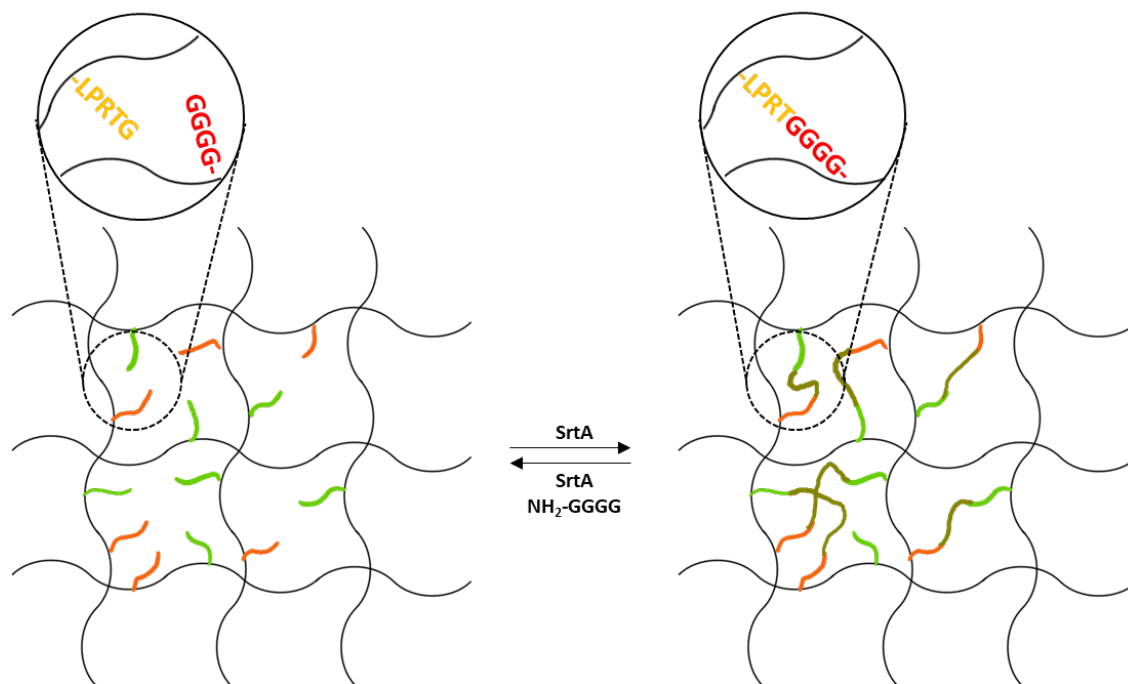
Fig. 4.18. Schematic of SrtA-mediate reversible stiffening of PEG-peptide hydrogels. Hydrogels were initially crosslinked via thiol-norbornene photoclick chemistry, stiffened through incubation with SrtA, and softened through incubation with SrtA and a N-terminal glycine-containing peptide.

To demonstrate the tunability of SrtA-mediated stiffening, PEG-peptide hydrogels (2.5 wt%, $R_{thiol:ene}$=1) containing SrtA substrates were incubated with varying time and concentrations of SrtA. (Fig. 4.19). As expected, the degree of stiffening increased with incubation time as the enzyme diffused into the hydrogel (Fig. 4.19B). The initial modulus (1 kPa) increased 1.75- to 2.5-fold in the presence of 25 μM of SrtA. However, further stiffening at later time points was not observed, indicating that 3 hours was sufficient for complete stiffening of the hydrogels. Additionally, the degree of stiffening is dependent on SrtA concentration. In particular, 2- to 4-fold increases in matrix stiffness were observed with SrtA concentrations from 10 to 50 μM and an incubation time of 4 hours. Taken together, these results demonstrate that pathophysiologically relevant degrees of stiffening [85, 86] can be achieved through SrtA-mediated peptide

ligation. The magnitude and timing of stiffening could be tuned by adjusting enzyme concentration and incubation time. Similar to the results in Section 4.2, gelation could be theoretically extended by lowering the enzyme concentration without changing other gel parameters.
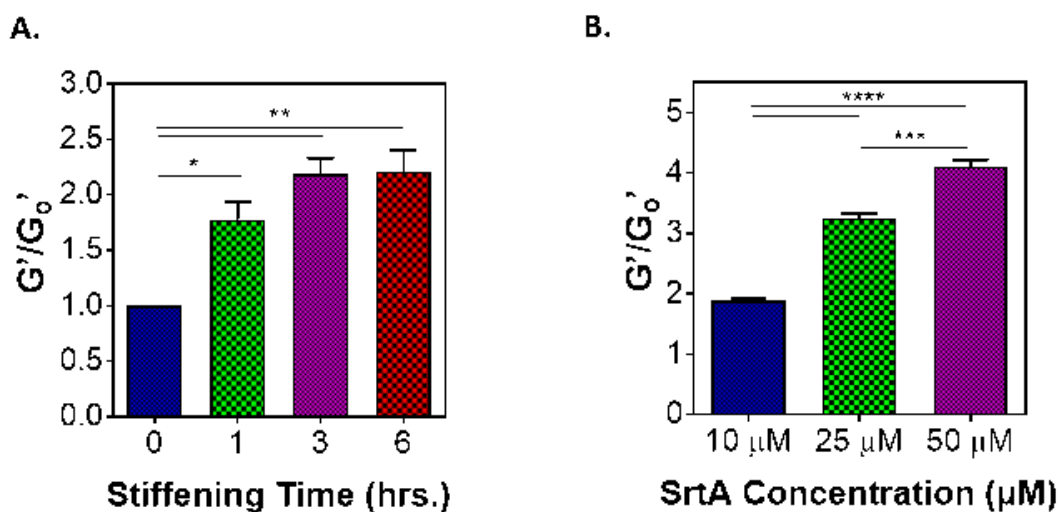
Fig. 4.19. (A) Effect of SrtA incubation time on stiffening of PEG-peptide hydrogels (2.5 wt%, $R_{thiol:ene} = 1$, 25 μM SrtA). (B) Effect of Srt conc. on stiffening of PEG-peptide hydrogels (2.5 wt%, $R_{thiol:ene} = 1$, 4 hr incubation).

After initially stiffening the hydrogels, matrix softening can occur in the presence of additional SrtA and soluble glycine substrate. As described in Figure 4.19, this could be tuned by adjusting incubation time and enzyme concentration. However, soluble glycine concentration could also influence the final modulus of the hydrogels (Fig. 4.20). Stiffened moduli (G'_{Stiff}, $\sim$3 kPa) were measured prior to incubation with SrtA (25 μM) and concentration of glycinamide (0, 2.5, 5, and 15 mM corresponding to 0, 0.5, 1, and 3-fold concentrations to crosslinker concentrations, respectively). After 4 hours of incubation, the final moduli were measured. Softening ranged from 0.8- to 0.5-fold with increasing concentrations of glycinamide. Interestingly, at a stoichiometric ratio of soluble and immobilized glycine (5 mM), minimal softening

was attained. Further, nearly full softening was achieved at a 3-fold concentration of soluble glycinamide. This is in line with literature suggesting high concentrations of glycinamide are required to drive full transpeptidation [85–87].

As mentioned previously, SrtA-mediated hydrolysis presents challenges to this strategy requiring extensive buffer replacement to remove residual SrtA and prevent this from occurring. However, it may be utilized to achieve gradual softening of the hydrogels (Fig. 4.20B). To demonstrate this, PEG-peptide hydrogels incubated with SrtA (25 μM) for 16 hours achieved full softening without the necessity of glycine. Again, softening could be extended by adjusting the enzyme concentration. However, it is important to note that this process is irreversible as the product LPRT-OH is generated rendering the peptide unreactive to the pendent glycine peptide.
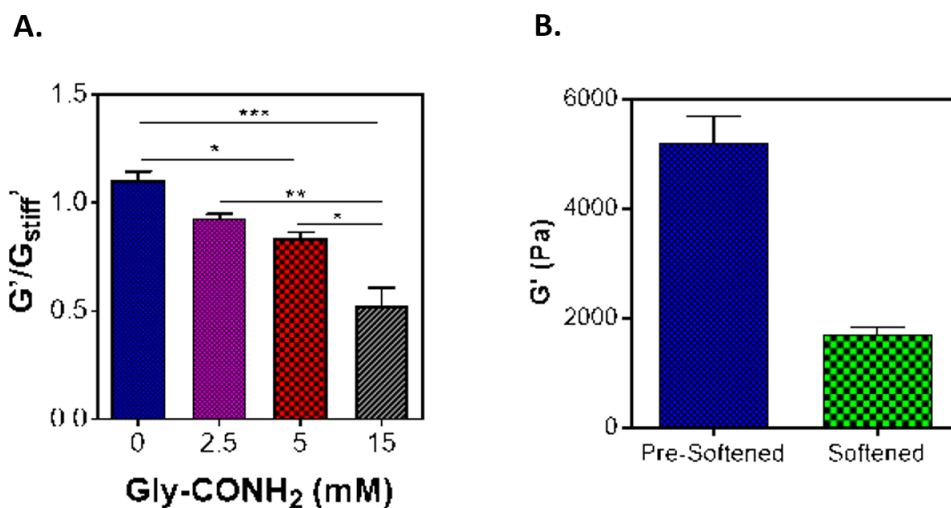
Fig. 4.20. (A) Effect of Gly-CONH$_2$ concentration on the softening of PEG-peptide hydrogels (2.5 wt%, R$_{thiol:ene}$ = 1, and 25 μM of SrtA). (B) SrtA-mediated hydrolytic degradation of PEG-peptide hydrogels (2.5 wt%, R$_{thiol:ene}$=1, 16 hour incubation time).

As shown in Figure 4.21, multiple cycles of stiffening and softening could be achieved. SrtA was added initially to create secondary crosslinks between pendent

LPRTG and GGGG. This covalent bond could be subsequently broken through the addition of SrtA and soluble Gly-CONH$_2$. The additional Gly-CONH$_2$ (at 3-fold concentration) competes with immobilized GGGG to regenerate the initial LPRTG and GGGG substrates. Interestingly, a slight increase in modulus occurred after removing the hydrogels from SrtA/glycinamide solution. This could be attributed to re-stiffening of the hydrogels caused by residual SrtA (i.e., reforming peptide bond between pendent LPRTG and GGG substrates). This dynamic crosslinking mechanism offers a wide range of the degree of stiffening and flexibility in the timescale of stiffening (i.e., hours to days).
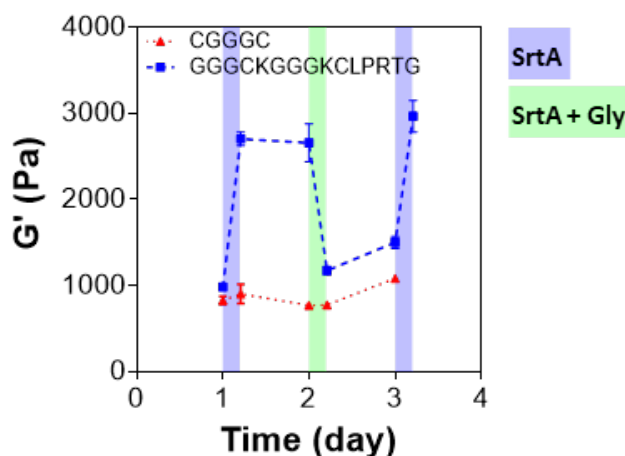
Fig. 4.21. Cyclic stiffening and softening of PEG-peptide hydrogels (2.5 wt%). Alternating 4-hour incubations with SrtA (25 μM) and SrtA with Gly-CONH$_2$ (15 mM) correspond to stiffening and softening, respectively.

4.10 Effect of SrtA-mediated Reversible Stiffening on COLO-357 Spheroid Formation.

To demonstrate the efficacy of this dynamically and enzymatically crosslinked hydrogel system as a platform for studying cell fate processes, COLO-357 cells were

encapsulated in the SrtA-stiffened/softened hydrogels. In particular, cells were initially encapsulated in hydrogels with elastic moduli of 1 or 3 kPa. These moduli were of biological relevance as 1 kPa and 3 kPa correspond to moduli of normal and desmoplastic pancreatic tissue, respectively [88, 89]. Cell laden hydrogels were fabricated with 2.5 wt% and 3.5 wt% of PEG8NB, which yielded gels with initial moduli of $\sim$1 kPa (i.e., soft gels) and $\sim$3 kPa (i.e., stiff gel), respectively. The 2.5 wt% PEG8NB hydrogels were treated with SrtA or SrtA with glycinamide to explore the effect of dynamic stiffening and softening on cell fate. Both initial thiol-norbornene photopolymerization and subsequent stiffening and softening (Fig. 4.22A) were cytocompatible as indicated by the high cell viability after each process (Fig. 4.22B). The diameters of cell spheroids were significantly smaller in statically stiff hydrogels compared with that in the soft gels. Spheroid growth was inhibited likely due to increasing crosslinking leading that restricted cell proliferation. After allowing spheroid proliferation for one week, the cell laden hydrogels were exposed to SrtA for 4 hours, which led to gel stiffening. The spheroid growth rate was similar to spheroids grown in statically stiff hydrogels ($\sim$3% change in diameter). Upon softening by 4-hour incubation with SrtA and glycinamide, spheroids growth resumed and matched more closely to the growth profile of cell spheroids grown in statically soft hydrogels ($\sim$15% change in diameter). This is likely due to the loosening of the hydrogel network permitting cell proliferation.
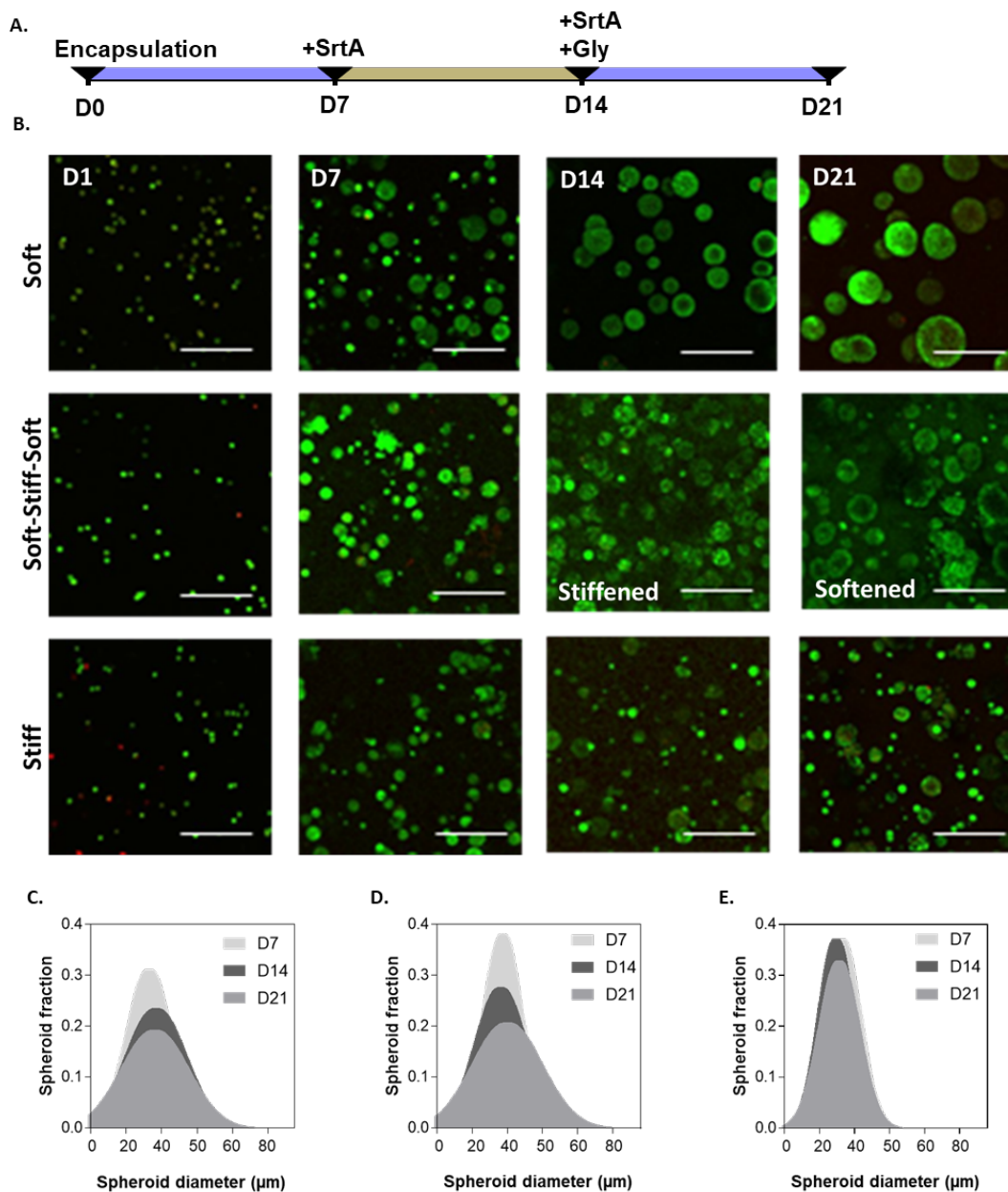
Fig. 4.22. (A) Timeline of reversible stiffening of cell laden hydrogels. Cells were allowed to grow in soft hydrogels prior to stiffening on day 7. Stiffened cell laden hydrogels were subsequently softened on day 14 and imaged on days 1, 7, 14, and 21. (B) Representative confocal images of encapsulated COLO-357 cells in statically soft and stiff as well as dynamically stiffened hydrogels. Histogram of spheroid diameters for (C) soft, (D) soft-stiff-soft, and (E) stiff hydrogels.

4.11 Effect of SrtA-mediated Matrix Stiffening on the Chemoresistance of COLO-357 Cells

Matrix stiffness has been reported to influence PDAC progression by affecting cell proliferation and chemoresistance [89]. To investigate the role of dynamic matrix stiffening on chemoresistance and EMT, COLO-357 cells were encapsulated in SrtA-mediated stiffening hydrogels and exposed to gemcitabine, a common PDAC therapeutic [90]. Cell laden hydrogels were exposed to SrtA treatment on day 3 post encapsulation, followed by gemcitabine treatment on day 7. As shown in Figure 4.23A, stiffened hydrogels inhibited spheroid growth while minimally affecting cell viability. Cell death was observed in soft (∼1 kPa storage modulus) and stiffened (∼4 kPa) hydrogels treated with gemcitabine compared with the non-treated soft control. However, the metabolic activity of cells within stiffened hydrogels remained unaffected by the gemcitabine treatment (Fig 4.23B). On the other hand, the metabolic activity of the cells in soft hydrogels significantly decreased suggesting gemcitabine both induced apoptosis and inhibited cell proliferation effectively in softer environments.
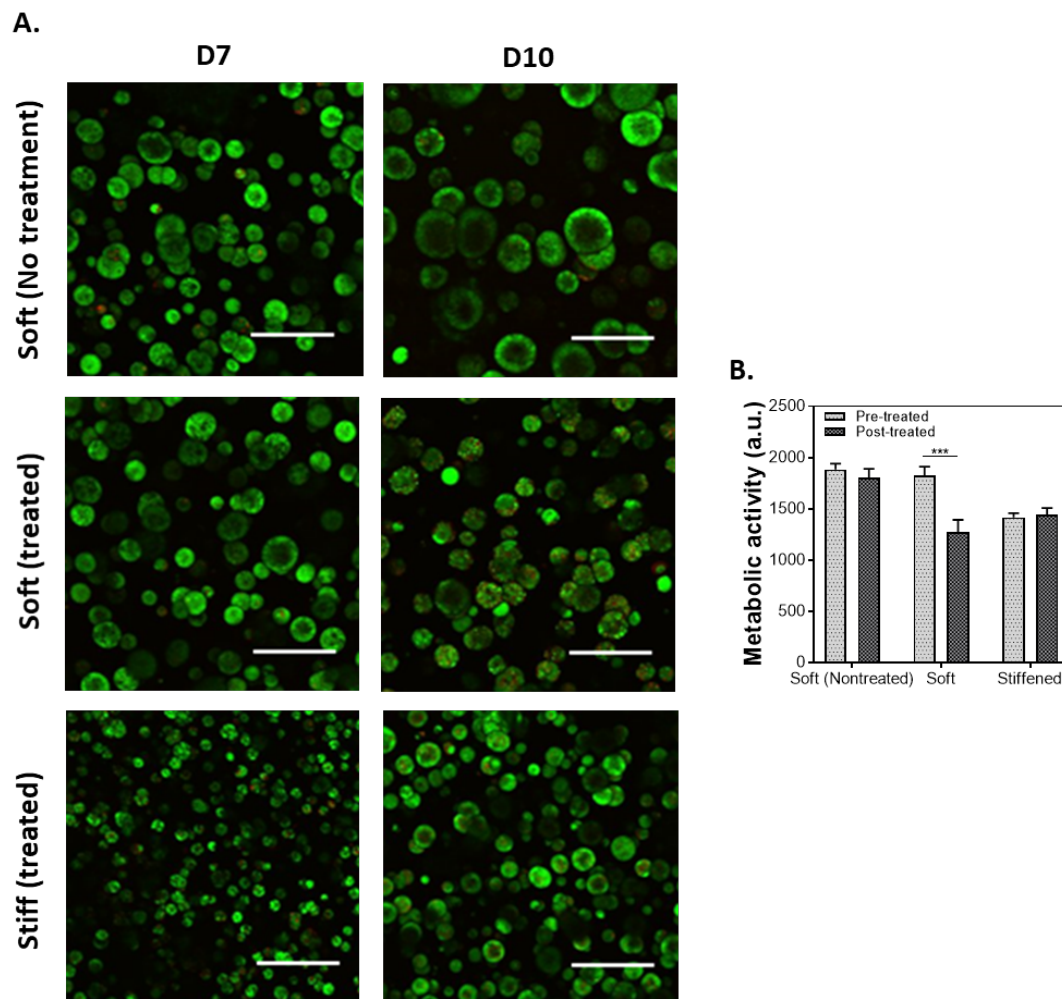
Fig. 4.23. (A) Representative images of COLO-357 cell-laden hydrogels with and without gemcitabine (1 μM) treatment. Hydrogels were incubated with SrtA on day 3, treated with gemcitabine on day 7 for three days, and imaged both day 7 and day 10 post-encapsulation. (B) Metabolic activity of encapsulated cells pre- (day 7) and post- (day 10) gemcitabine treatment (N = 6).

In addition to cell viability, the expression of chemoresistance-associated gene sonic hedgehog (SHH) and YAP target gene ankyrin repeat domain 1 (ANKRD1) were evaluated after gemcitabine treatment. As shown in Figure 4.24, the enzyme-

induced stiffening up-regulated the expression of SHH and ANKRD1 ($\sim$5 and $\sim$70-fold, respectively) in the cells compared with the control group.
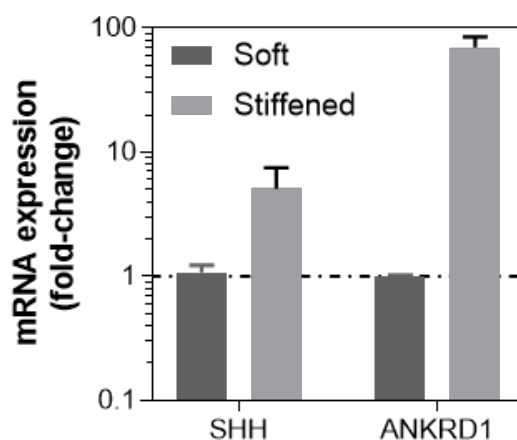
Fig. 4.24. SHH and ANKRD1 expression in COLO-357 cells encapsulated in soft and stiffened hydrogels treated with gemcitabine (1 μM) for three days (Mean $\pm$ SEM, N=4).

SHH was detected due to its role in tumor size control, CSC stemness, and chemotherapy resistance [91]. Mechanistically, expression of SHH promotes drug efflux through multi-drug resistance-1 (MDR1) expression [92]. Furthermore, SHH has been implicated in pre-invasive and invasive phenotypes of PDAC [93], oncogenic Kras expression [94], and Smo-dependent signaling [95]. Both Kras and Smo-dependent signaling are significant drivers of pancreatic neoplasia by promoting proliferation, anti-apoptosis, and tumor environment remodeling [96–98]. Matrix stiffening also enhances EMT through the YAP/TAZ signaling pathway [89]. The up-regulation of ANKRD1 expression is consistent with other reports suggesting YAP and TAZ localization increases with matrix stiffening [99]. Furthermore, gemcitabine may be preventing tumor suppressor kinase LATS1/2 inhibition of YAP/TAZ by its nucleoside analogue activity [100]. However, further research is required to characterize the

effect of gemcitabine on LATS1/2 activity. Taken together, these data suggest matrix stiffening influences the survival, proliferation, and gene expression of pancreatic cancer cells through SHH and YAP/TAZ signaling.

5. SUMMARY AND RECOMMENDATIONS

5.1 Summary

In summary, dynamic enzymatically-crosslinked hydrogels were prepared using SrtA-mediated transpeptidation and thiol-norbornene photo-click chemistry. The biophysical properties of the hydrogels can be temporally tuned independent of hydrogel formulation through MT-mediated dityrosine formation and SrtA-mediated transpeptidation. SrtA-mediated crosslinked hydrogels provide highly cytcompatible cell culture platforms by promoting cell viability, proliferation and morphogenesis in 3D. Moreover, the hydrogels can be rapidly and site-specifically degraded in the presence of additional SrtA and glycine. MT-mediated dityrosine formation proved to be an efficient and cytocompatible chemistry for pathophysiologically relevant degrees of stiffening. In addition to MT-mediated matrix stiffening, SrtA-mediated reversible stiffening of thiol-ene hydrogels could be achieved by incorporating pendent SrtA substrates. Both matrix stiffening and softening could be tuned by adjusting hydrogel formulation, enzyme, and soluble glycine concentration.

5.2 Recommendations

Although protease sensitive crosslinkers and cell adhesion ligands were not incorporated in this study, future work could include the incorporation of bioactive peptides (e.g., RGDS or MMP-sensitive linker, GPQGIWGQ) to permit cell-driven adhesion and degradation. Further, pendent moieties could be attached or removed by simply incorporating the SrtA substrate, LPXTG or G_n, to the peptide or protein (e.g., GGG-RGD). This could be utilized not only to study the effect of matrix stiffening/softening, but also the role of temporally dependent ligand presentation on

cell fate processes. Due to the orthogonality of both thiol-ene and SrtA-mediated crosslinking, natural materials (e.g., gelatin and heparin) could be incorporated, further enhancing the biological relevancy of the hydrogels.

The reversibility of SrtA transpeptidation is both an advantage and a limitation, depending on the application. If necessary, the reaction can be rendered irreversible by synthesizing depsipeptide substrates or peptides that fragment to form an unreactive diketopiperazine moiety [101, 102]. This would mitigate the necessity for excess glycine substrate and would be particularly useful in applications requiring high-value or minimal reagents for modification. On the other hand, the reversibility may be desirable for site specific degradation of hydrogels. While this thesis work demonstrated the degradability of the SrtA-mediated crosslinked hydrogels, a proper application was not explored. Therefore, another avenue of future work could be using this degradable crosslinking mechanism to generate and recover tumor spheroids for future functional and biological characterization studies.

Finally, future studies involving the use of reversible SrtA-mediated stiffening to further characterize PDAC cells in temporally dynamic matrices should be completed. Bioactive molecules present in the PDAC desmoplasia such as hyaluronic acid [103, 104] should be incorporated to study the synergistic effect of biophysical and biochemical components driving EMT, mesenchymal to epithelial transition (MET), and chemotherapeutic resistance.

LIST OF REFERENCES

LIST OF REFERENCES

[1] L. Macri-Pellizzeri, B. Pelacho, A. Sancho, O. Iglesias-Garcia, A. M. Simon-Yarza, M. Soriano-Navarro, S. Gonzalez-Granero, J. M. Garcia-Verdugo, E. M. De-Juan-Pardo, and F. Prosper, "Substrate stiffness and composition specifically direct differentiation of induced pluripotent stem cells," *Tissue Eng Part A*, vol. 21, no. 9-10, pp. 1633–41, 2015.

[2] M. Schober, R. Jesenofsky, R. Faissner, C. Weidenauer, W. Hagmann, P. Michl, R. L. Heuchel, S. L. Haas, and J. M. Lohr, "Desmoplasia and chemoresistance in pancreatic cancer," *Cancers (Basel)*, vol. 6, no. 4, pp. 2137–54, 2014.

[3] R. G. Wells, "Tissue mechanics and fibrosis," *Biochim Biophys Acta*, vol. 1832, no. 7, pp. 884–90, 2013.

[4] F. Bordeleau, B. N. Mason, E. M. Lollis, M. Mazzola, M. R. Zanotelli, S. Somasegar, J. P. Califano, C. Montague, D. J. LaValley, J. Huynh, N. Mencia-Trinchant, Y. L. Negron Abril, D. C. Hassane, L. J. Bonassar, J. T. Butcher, R. S. Weiss, and C. A. Reinhart-King, "Matrix stiffening promotes a tumor vasculature phenotype," *Proc Natl Acad Sci U S A*, vol. 114, no. 3, pp. 492–497.

[5] D. T. Butcher, T. Alliston, and V. M. Weaver, "A tense situation: forcing tumour progression," *Nat Rev Cancer*, vol. 9, no. 2, pp. 108–22, 2009.

[6] N. Gjorevski, N. Sachs, A. Manfrin, S. Giger, M. E. Bragina, P. Ordonez-Moran, H. Clevers, and M. P. Lutolf, "Designer matrices for intestinal stem cell and organoid culture," *Nature*, vol. 539, no. 7630, pp. 560–564, 2016.

[7] K. E. Sullivan, K. P. Quinn, K. M. Tang, I. Georgakoudi, and r. Black, L. D., "Extracellular matrix remodeling following myocardial infarction influences the therapeutic potential of mesenchymal stem cells," *Stem Cell Res Ther*, vol. 5, no. 1, p. 14, 2014.

[8] Y. Liang, N. E. Clay, K. M. Sullivan, J. Leong, A. Ozcelikkale, M. H. Rich, M. K. Lee, M. H. Lai, H. Jeon, B. Han, Y. W. Tong, and H. Kong, "Enzyme-induced matrix softening regulates hepatocarcinoma cancer cell phenotypes," *Macromol Biosci*, vol. 17, no. 9, 2017.

[9] O. Eickelberg, E. Kohler, F. Reichenberger, S. Bertschin, T. Woodtli, P. Erne, A. P. Perruchoud, and M. Roth, "Extracellular matrix deposition by primary human lung fibroblasts in response to tgf-beta1 and tgf-beta3," *Am J Physiol*, vol. 276, no. 5 Pt 1, pp. L814–24, 1999.

[10] P. Kumar, A. Satyam, D. Cigognini, A. Pandit, and D. I. Zeugolis, "Low oxygen tension and macromolecular crowding accelerate extracellular matrix deposition in human corneal fibroblast culture," *J Tissue Eng Regen Med*, 2016.

[11] G. S. Baroni, L. D'Ambrosio, P. Curto, A. Casini, R. Mancini, A. M. Jezequel, and A. Benedetti, "Interferon gamma decreases hepatic stellate cell activation and extracellular matrix deposition in rat liver fibrosis," *Hepatology*, vol. 23, no. 5, pp. 1189–99, 1996.

[12] R. C. Siegel, S. R. Pinnell, and G. R. Martin, "Cross-linking of collagen and elastin. properties of lysyl oxidase," *Biochemistry*, vol. 9, no. 23, pp. 4486–92, 1970.

[13] M. Perepelyuk, M. Terajima, A. Y. Wang, P. C. Georges, P. A. Janmey, M. Ya-mauchi, and R. G. Wells, "Hepatic stellate cells and portal fibroblasts are the major cellular sources of collagens and lysyl oxidases in normal liver and early after injury," *Am J Physiol Gastrointest Liver Physiol*, vol. 304, no. 6, pp. G605–14, 2013.

[14] P. Lu, K. Takai, V. M. Weaver, and Z. Werb, "Extracellular matrix degradation and remodeling in development and disease," *Cold Spring Harb Perspect Biol*, vol. 3, no. 12, 2011.

[15] M. Hidalgo, S. Cascinu, J. Kleeff, R. Labianca, J. M. Lohr, J. Neoptolemos, F. X. Real, J. L. Van Laethem, and V. Heinemann, "Addressing the challenges of pancreatic cancer: future directions for improving outcomes," *Pancreatology*, vol. 15, no. 1, pp. 8–18, 2015. [Online]. Available: https://www.ncbi.nlm.nih.gov/pubmed/25547205

[16] A. Vincent, J. Herman, R. Schulick, R. H. Hruban, and M. Goggins, "Pancreatic cancer," *Lancet*, vol. 378, no. 9791, pp. 607–20, 2011.

[17] A. N. Shah, J. M. Summy, J. Zhang, S. I. Park, N. U. Parikh, and G. E. Gallick, "Development and characterization of gemcitabine-resistant pancreatic tumor cells," *Ann Surg Oncol*, vol. 14, no. 12, pp. 3629–37, 2007.

[18] T. Reya, S. J. Morrison, M. F. Clarke, and I. L. Weissman, "Stem cells, cancer, and cancer stem cells," *Nature*, vol. 414, no. 6859, pp. 105–11, 2001.

[19] D. J. Drasin, T. P. Robin, and H. L. Ford, "Breast cancer epithelial-to-mesenchymal transition: examining the functional consequences of plasticity," *Breast Cancer Res*, vol. 13, no. 6, p. 226, 2011.

[20] K. Kikuta, A. Masamune, T. Watanabe, H. Ariga, H. Itoh, S. Hamada, K. Satoh, S. Egawa, M. Unno, and T. Shimosegawa, "Pancreatic stellate cells promote epithelial-mesenchymal transition in pancreatic cancer cells," *Biochem Biophys Res Commun*, vol. 403, no. 3-4, pp. 380–4, 2010.

[21] E. Jabbari, S. K. Sarvestani, L. Daneshian, and S. Moeinzadeh, "Optimum 3d matrix stiffness for maintenance of cancer stem cells is dependent on tissue origin of cancer cells," *PLoS One*, vol. 10, no. 7, p. e0132377, 2015.

[22] Y. You, Q. Zheng, Y. Dong, X. Xie, Y. Wang, S. Wu, L. Zhang, Y. Wang, T. Xue, Z. Wang, R. Chen, Y. Wang, J. Cui, and Z. Ren, "Matrix stiffness-mediated effects on stemness characteristics occurring in hcc cells," *Oncotarget*, vol. 7, no. 22, pp. 32 221–31, 2016.

[23] J. W. Shin and D. J. Mooney, "Extracellular matrix stiffness causes systematic variations in proliferation and chemosensitivity in myeloid leukemias," *Proc Natl Acad Sci U S A*, vol. 113, no. 43, pp. 12 126–12 131, 2016.

[24] A. Marinkovic, J. D. Mih, J. A. Park, F. Liu, and D. J. Tschumperlin, "Improved throughput traction microscopy reveals pivotal role for matrix stiffness in fibroblast contractility and tgf-beta responsiveness," *Am J Physiol Lung Cell Mol Physiol*, vol. 303, no. 3, pp. L169–80, 2012.

[25] J. H. Chen, W. L. Chen, K. L. Sider, C. Y. Yip, and C. A. Simmons, "beta-catenin mediates mechanically regulated, transforming growth factor-beta1-induced myofibroblast differentiation of aortic valve interstitial cells," *Arterioscler Thromb Vasc Biol*, vol. 31, no. 3, pp. 590–7, 2011.

[26] C. Huang, S. Akaishi, and R. Ogawa, "Mechanosignaling pathways in cutaneous scarring," *Arch Dermatol Res*, vol. 304, no. 8, pp. 589–97, 2012.

[27] F. Liu, J. D. Mih, B. S. Shea, A. T. Kho, A. S. Sharif, A. M. Tager, and D. J. Tschumperlin, "Feedback amplification of fibrosis through matrix stiffening and cox-2 suppression," *J Cell Biol*, vol. 190, no. 4, pp. 693–706, 2010.

[28] M. C. Lampi and C. A. Reinhart-King, "Targeting extracellular matrix stiffness to attenuate disease: From molecular mechanisms to clinical trials," *Sci Transl Med*, vol. 10, no. 422, 2018.

[29] A. J. Engler, S. Sen, H. L. Sweeney, and D. E. Discher, "Matrix elasticity directs stem cell lineage specification," *Cell*, vol. 126, no. 4, pp. 677–89, 2006.

[30] J. E. Dixon, D. A. Shah, C. Rogers, S. Hall, N. Weston, C. D. Parmenter, D. McNally, C. Denning, and K. M. Shakesheff, "Combined hydrogels that switch human pluripotent stem cells from self-renewal to differentiation," *Proc Natl Acad Sci U S A*, vol. 111, no. 15, pp. 5580–5, 2014.

[31] M. Guvendiren and J. A. Burdick, "Stiffening hydrogels to probe short- and long-term cellular responses to dynamic mechanics," *Nat Commun*, vol. 3, p. 792, 2012.

[32] R. S. Stowers, S. C. Allen, and L. J. Suggs, "Dynamic phototuning of 3d hydrogel stiffness," *Proc Natl Acad Sci U S A*, vol. 112, no. 7, pp. 1953–8, 2015.

[33] . N. B. G. Szilgyi and A., "Reversible disulphide formation in polymer networks: A versatile functional group from synthesis to applications," *European Polymer Journal*, vol. 49, no. 6, pp. 1268–1286, 2013.

[34] H. Y. Liu, T. Greene, T. Y. Lin, C. S. Dawes, M. Korc, and C. C. Lin, "Enzyme-mediated stiffening hydrogels for probing activation of pancreatic stellate cells," *Acta Biomater*, vol. 48, pp. 258–269, 2017.

[35] S. R. Caliari, M. Perepelyuk, E. M. Soulas, G. Y. Lee, R. G. Wells, and J. A. Burdick, "Gradually softening hydrogels for modeling hepatic stellate cell behavior during fibrosis regression," *Integr Biol (Camb)*, vol. 8, no. 6, pp. 720–8, 2016.

[36] S. P. Zustiak and J. B. Leach, "Hydrolytically degradable poly(ethylene glycol) hydrogel scaffolds with tunable degradation and mechanical properties," *Biomacromolecules*, vol. 11, no. 5, pp. 1348–57, 2010.

[37] A. M. Kloxin, A. M. Kasko, C. N. Salinas, and K. S. Anseth, "Photodegradable hydrogels for dynamic tuning of physical and chemical properties," *Science*, vol. 324, no. 5923, pp. 59–63, 2009.

[38] L. Shi, Y. Zhang, and D. Ossipov, "Enzymatic degradation of hyaluronan hydrogels with different capacity for in situ bio-mineralization," *Biopolymers*, vol. 109, no. 2, 2018.

[39] A. M. Rosales, K. M. Mabry, E. M. Nehls, and K. S. Anseth, "Photoresponsive elastic properties of azobenzene-containing poly(ethylene-glycol)-based hydrogels," *Biomacromolecules*, vol. 16, no. 3, pp. 798–806, 2015.

[40] A. M. Rosales, S. L. Vega, F. W. DelRio, J. A. Burdick, and K. S. Anseth, "Hydrogels with reversible mechanics to probe dynamic cell microenvironments," *Angew Chem Int Ed Engl*, vol. 56, no. 40, pp. 12 132–12 136, 2017.

[41] H. Shih and C. Lin, "Tuning stiffness of cell-laden hydrogel via host-guest interactions," *Journal of Materials Chemistry B*, vol. 4, no. 29, pp. 4969–4974, 2016.

[42] H. W. W. W. W. X. B. X. D. L. Y. Q. M. Wu, X and F. Sun, "Reversible hydrogels with tunable mechanical properties for optically controlling cell migration," *Nano Research*, 2017.

[43] A. Metters and J. Hubbell, "Network formation and degradation behavior of hydrogels formed by michael-type addition reactions," *Biomacromolecules*, vol. 6, no. 1, pp. 290–301, 2005.

[44] M. A. Rice, J. Sanchez-Adams, and K. S. Anseth, "Exogenously triggered, enzymatic degradation of photopolymerized hydrogels with polycaprolactone subunits: experimental observation and modeling of mass loss behavior," *Biomacromolecules*, vol. 7, no. 6, pp. 1968–75, 2006.

[45] J. West and H. JA, "Polymeric biomaterials with degradation sites for proteases involved in cell migration," *Macromolecules*, vol. 32, no. 1, pp. 241–244, 1999.

[46] B. Trappmann, B. M. Baker, W. J. Polacheck, C. K. Choi, J. A. Burdick, and C. S. Chen, "Matrix degradability controls multicellularity of 3d cell migration," *Nat Commun*, vol. 8, no. 1, p. 371, 2017.

[47] A. M. Rosales, C. B. Rodell, M. H. Chen, M. G. Morrow, K. S. Anseth, and J. A. Burdick, "Reversible control of network properties in azobenzene-containing hyaluronic acid-based hydrogels," *Bioconjug Chem*, 2018.

[48] I. N. Lee, O. Dobre, D. Richards, C. Ballestrem, J. M. Curran, J. A. Hunt, S. M. Richardson, J. Swift, and L. S. Wong, "Photoresponsive hydrogels with photoswitchable mechanical properties allow time-resolved analysis of cellular responses to matrix stiffening," *ACS Appl Mater Interfaces*, 2018.

[49] J. J. Roberts, P. Naudiyal, K. S. Lim, L. A. Poole-Warren, and P. J. Martens, "A comparative study of enzyme initiators for crosslinking phenol-functionalized hydrogels for cell encapsulation," *Biomater Res*, vol. 20, p. 30, 2016.

[50] D. Huber, G. Tegl, M. Baumann, E. Sommer, E. G. Gorji, N. Borth, G. Schleining, G. S. Nyanhongo, and G. M. Guebitz, "Chitosan hydrogel formation using laccase activated phenolics as cross-linkers," *Carbohydr Polym*, vol. 157, pp. 814–822, 2017.

[51] F. Anjum, P. S. Lienemann, S. Metzger, J. Biernaskie, M. S. Kallos, and M. Ehrbar, "Enzyme responsive gag-based natural-synthetic hybrid hydrogel for tunable growth factor delivery and stem cell differentiation," *Biomaterials*, vol. 87, pp. 104–117, 2016.

[52] E. Cambria, K. Renggli, C. C. Ahrens, C. D. Cook, C. Kroll, A. T. Krueger, B. Imperiali, and L. G. Griffith, "Covalent modification of synthetic hydrogels with bioactive proteins via sortase-mediated ligation," *Biomacromolecules*, vol. 16, no. 8, pp. 2316–26, 2015.

[53] N. Z. Alarake, P. Frohberg, T. Groth, and M. Pietzsch, "Mechanical properties and biocompatibility of in situ enzymatically cross-linked gelatin hydrogels," *Int J Artif Organs*, vol. 40, no. 4, pp. 159–168, 2017.

[54] A. Ranga, M. P. Lutolf, J. Hilborn, and D. A. Ossipov, "Hyaluronic acid hydrogels formed in situ by transglutaminase-catalyzed reaction," *Biomacromolecules*, vol. 17, no. 5, pp. 1553–60, 2016.

[55] G. Rocasalbas, A. Francesko, S. Tourino, X. Fernandez-Francos, G. M. Guebitz, and T. Tzanov, "Laccase-assisted formation of bioactive chitosan/gelatin hydrogel stabilized with plant polyphenols," *Carbohydr Polym*, vol. 92, no. 2, pp. 989–96, 2013.

[56] K. A. Mosiewicz, K. Johnsson, and M. P. Lutolf, "Phosphopantetheinyl transferase-catalyzed formation of bioactive hydrogels for tissue engineering," *J Am Chem Soc*, vol. 132, no. 17, pp. 5972–4, 2010.

[57] O. B. Ayyub and P. Kofinas, "Enzyme induced stiffening of nanoparticle-hydrogel composites with structural color," *ACS Nano*, vol. 9, no. 8, pp. 8004–11, 2015.

[58] C. N. Salinas and K. S. Anseth, "The enhancement of chondrogenic differentiation of human mesenchymal stem cells by enzymatically regulated rgd functionalities," *Biomaterials*, vol. 29, no. 15, pp. 2370–7, 2008.

[59] E. A. Phelps, K. L. Templeman, P. M. Thule, and A. J. Garcia, "Engineered vegf-releasing peg-mal hydrogel for pancreatic islet vascularization," *Drug Deliv Transl Res*, vol. 5, no. 2, pp. 125–36, 2015.

[60] E. J. Land, C. A. Ramsden, and P. A. Riley, "Tyrosinase autoactivation and the chemistry of ortho-quinone amines," *Acc Chem Res*, vol. 36, no. 5, pp. 300–8, 2003.

[61] M. R. Arkenberg and C. C. Lin, "Orthogonal enzymatic reactions for rapid crosslinking and dynamic tuning of peg-peptide hydrogels," *Biomater Sci*, vol. 5, no. 11, pp. 2231–2240, 2017.

[62] H. Y. Liu, M. Korc, and C. C. Lin, "Biomimetic and enzyme-responsive dynamic hydrogels for studying cell-matrix interactions in pancreatic ductal adenocarcinoma," *Biomaterials*, vol. 160, pp. 24–36, 2018.

[63] S. H. Kim, Y. H. An, H. D. Kim, K. Kim, S. H. Lee, H. G. Yim, B. G. Kim, and N. S. Hwang, "Enzyme-mediated tissue adhesive hydrogels for meniscus repair," *Int J Biol Macromol*, 2017.

[64] M. W. Popp and H. L. Ploegh, "Making and breaking peptide bonds: protein engineering using sortase," *Angew Chem Int Ed Engl*, vol. 50, no. 22, pp. 5024–32, 2011.

[65] B. M. Paterson, K. Alt, C. M. Jeffery, R. I. Price, S. Jagdale, S. Rigby, C. C. Williams, K. Peter, C. E. Hagemeyer, and P. S. Donnelly, "Enzyme-mediated site-specific bioconjugation of metal complexes to proteins: sortase-mediated coupling of copper-64 to a single-chain antibody," *Angew Chem Int Ed Engl*, vol. 53, no. 24, pp. 6115–9, 2014.

[66] L. K. Swee, C. P. Guimaraes, S. Sehrawat, E. Spooner, M. I. Barrasa, and H. L. Ploegh, "Sortase-mediated modification of alphadec205 affords optimization of antigen presentation and immunization against a set of viral epitopes," *Proc Natl Acad Sci U S A*, vol. 110, no. 4, pp. 1428–33, 2013.

[67] Z. Wu, X. Guo, and Z. Guo, "Sortase a-catalyzed peptide cyclization for the synthesis of macrocyclic peptides and glycopeptides," *Chem Commun (Camb)*, vol. 47, no. 32, pp. 9218–20, 2011.

[68] A. T. Krueger, C. Kroll, E. Sanchez, L. G. Griffith, and B. Imperiali, "Tailoring chimeric ligands for studying and biasing erbb receptor family interactions," *Angew Chem Int Ed Engl*, vol. 53, no. 10, pp. 2662–6, 2014.

[69] J. Valdez, C. D. Cook, C. C. Ahrens, A. J. Wang, A. Brown, M. Kumar, L. Stockdale, D. Rothenberg, K. Renggli, E. Gordon, D. Lauffenburger, F. White, and L. Griffith, "On-demand dissolution of modular, synthetic extracellular matrix reveals local epithelial-stromal communication networks," *Biomaterials*, vol. 130, pp. 90–103, 2017.

[70] C. Deane, "Bioorthogonal chemistry: Click on, click off," *Nat Chem Biol*, vol. 13, no. 10, p. 1057, 2017.

[71] C. C. Lin, C. S. Ki, and H. Shih, "Thiol-norbornene photo-click hydrogels for tissue engineering applications," *J Appl Polym Sci*, vol. 132, no. 8, 2015.

[72] C. C. Lin, A. Raza, and H. Shih, "Peg hydrogels formed by thiol-ene photo-click chemistry and their effect on the formation and recovery of insulin-secreting cell spheroids," *Biomaterials*, vol. 32, no. 36, pp. 9685–95, 2011.

[73] J. D. McCall and K. S. Anseth, "Thiol-ene photopolymerizations provide a facile method to encapsulate proteins and maintain their bioactivity," *Biomacromolecules*, vol. 13, no. 8, pp. 2410–7, 2012.

[74] B. V. Sridhar, J. L. Brock, J. S. Silver, J. L. Leight, M. A. Randolph, and K. S. Anseth, "Development of a cellularly degradable peg hydrogel to promote articular cartilage extracellular matrix deposition," *Adv Healthc Mater*, vol. 4, no. 5, pp. 702–13, 2015.

[75] B. D. Fairbanks, M. P. Schwartz, A. E. Halevi, C. R. Nuttelman, C. N. Bowman, and K. S. Anseth, "A versatile synthetic extracellular matrix mimic via thiol-norbornene photopolymerization," *Adv Mater*, vol. 21, no. 48, pp. 5005–5010, 2009.

[76] B. D. Fairbanks, M. P. Schwartz, C. N. Bowman, and K. S. Anseth, "Photoinitiated polymerization of peg-diacrylate with lithium phenyl-2,4,6-trimethylbenzoylphosphinate: polymerization rate and cytocompatibility," *Biomaterials*, vol. 30, no. 35, pp. 6702–7, 2009.

[77] C. P. Guimaraes, M. D. Witte, C. S. Theile, G. Bozkurt, L. Kundrat, A. E. Blom, and H. L. Ploegh, "Site-specific c-terminal and internal loop labeling of proteins using sortase-mediated reactions," *Nat Protoc*, vol. 8, no. 9, pp. 1787–99, 2013.

[78] H. Hirakawa, S. Ishikawa, and T. Nagamune, "Ca2+ -independent sortase-a exhibits high selective protein ligation activity in the cytoplasm of escherichia coli," *Biotechnol J*, vol. 10, no. 9, pp. 1487–92, 2015.

[79] I. Chen, B. M. Dorr, and D. R. Liu, "A general strategy for the evolution of bond-forming enzymes using yeast display," *Proc Natl Acad Sci U S A*, vol. 108, no. 28, pp. 11 399–404, 2011.

[80] M. D. Witte, T. Wu, C. P. Guimaraes, C. S. Theile, A. E. Blom, J. R. Ingram, Z. Li, L. Kundrat, S. D. Goldberg, and H. L. Ploegh, "Site-specific protein modification using immobilized sortase in batch and continuous-flow systems," *Nat Protoc*, vol. 10, no. 3, pp. 508–16, 2015.

[81] X. Huang, A. Aulabaugh, W. Ding, B. Kapoor, L. Alksne, K. Tabei, and G. Ellestad, "Kinetic mechanism of staphylococcus aureus sortase srta," *Biochemistry*, vol. 42, no. 38, pp. 11 307–15, 2003.

[82] C. C. Lin and K. S. Anseth, "Cell-cell communication mimicry with poly(ethylene glycol) hydrogels for enhancing beta-cell function," *Proc Natl Acad Sci U S A*, vol. 108, no. 16, pp. 6380–5, 2011.

[83] A. Raza and C. C. Lin, "Generation and recovery of beta-cell spheroids from step-growth peg-peptide hydrogels," *J Vis Exp*, no. 70, p. e50081, 2012.

[84] H. Shih, T. Greene, M. Korc, and C. C. Lin, "Modular and adaptable tumor niche prepared from visible light initiated thiol-norbornene photopolymerization," *Biomacromolecules*, vol. 17, no. 12, pp. 3872–3882, 2016.

[85] H. Mao, S. A. Hart, A. Schink, and B. A. Pollok, "Sortase-mediated protein ligation: a new method for protein engineering," *J Am Chem Soc*, vol. 126, no. 9, pp. 2670–1, 2004.

[86] N. Hirota, D. Yasuda, T. Hashidate, T. Yamamoto, S. Yamaguchi, T. Nagamune, T. Nagase, T. Shimizu, and M. Nakamura, "Amino acid residues critical for endoplasmic reticulum export and trafficking of platelet-activating factor receptor," *J Biol Chem*, vol. 285, no. 8, pp. 5931–40, 2010.

[87] T. Yamamoto and T. Nagamune, "Expansion of the sortase-mediated labeling method for site-specific n-terminal labeling of cell surface proteins on living cells," *Chem Commun (Camb)*, no. 9, pp. 1022–4, 2009.

[88] A. V. Nguyen, K. D. Nyberg, M. B. Scott, A. M. Welsh, A. H. Nguyen, N. Wu, S. V. Hohlbauch, N. A. Geisse, E. A. Gibb, A. G. Robertson, T. R. Donahue, and A. C. Rowat, "Stiffness of pancreatic cancer cells is associated with increased invasive potential," *Integr Biol (Camb)*, vol. 8, no. 12, pp. 1232–1245, 2016.

[89] A. J. Rice, E. Cortes, D. Lachowski, B. C. H. Cheung, S. A. Karim, J. P. Morton, and A. Del Rio Hernandez, "Matrix stiffness induces epithelial-mesenchymal transition and promotes chemoresistance in pancreatic cancer cells," *Oncogenesis*, vol. 6, no. 7, p. e352, 2017.

[90] M. Amrutkar and I. P. Gladhaug, "Pancreatic cancer chemoresistance to gemcitabine," *Cancers (Basel)*, vol. 9, no. 11, 2017.

[91] M. Lauth and R. Toftgard, "Hedgehog signaling and pancreatic tumor development," *Adv Cancer Res*, vol. 110, pp. 1–17, 2011.

[92] J. Sims-Mourtada, J. G. Izzo, J. Ajani, and K. S. Chao, "Sonic hedgehog promotes multiple drug resistance by regulation of drug transport," *Oncogene*, vol. 26, no. 38, pp. 5674–9, 2007.

[93] H. Nakashima, M. Nakamura, H. Yamaguchi, N. Yamanaka, T. Akiyoshi, K. Koga, K. Yamaguchi, M. Tsuneyoshi, M. Tanaka, and M. Katano, "Nuclear factor-kappab contributes to hedgehog signaling pathway activation through sonic hedgehog induction in pancreatic cancer," *Cancer Res*, vol. 66, no. 14, pp. 7041–9, 2006.

[94] J. Ling, Y. Kang, R. Zhao, Q. Xia, D. F. Lee, Z. Chang, J. Li, B. Peng, J. B. Fleming, H. Wang, J. Liu, I. R. Lemischka, M. C. Hung, and P. J. Chiao, "Krasg12d-induced ikk2/beta/nf-kappab activation by il-1alpha and p62 feedforward loops is required for development of pancreatic ductal adenocarcinoma," *Cancer Cell*, vol. 21, no. 1, pp. 105–20, 2012.

[95] J. M. Bailey, A. M. Mohr, and M. A. Hollingsworth, "Sonic hedgehog paracrine signaling regulates metastasis and lymphangiogenesis in pancreatic cancer," *Oncogene*, vol. 28, no. 40, pp. 3513–25, 2009.

[96] S. Eser, A. Schnieke, G. Schneider, and D. Saur, "Oncogenic kras signalling in pancreatic cancer," *Br J Cancer*, vol. 111, no. 5, pp. 817–22, 2014.

[97] O. Nolan-Stevaux, J. Lau, M. L. Truitt, G. C. Chu, M. Hebrok, M. E. Fernandez-Zapico, and D. Hanahan, "Gli1 is regulated through smoothened-independent mechanisms in neoplastic pancreatic ducts and mediates pdac cell survival and transformation," *Genes Dev*, vol. 23, no. 1, pp. 24–36, 2009.

[98] Y. Bai, Y. Bai, J. Dong, Q. Li, Y. Jin, B. Chen, and M. Zhou, "Hedgehog signaling in pancreatic fibrosis and cancer," *Medicine (Baltimore)*, vol. 95, no. 10, p. e2996, 2016.

[99] F. Zanconato, G. Battilana, M. Cordenonsi, and S. Piccolo, "Yap/taz as therapeutic targets in cancer," *Curr Opin Pharmacol*, vol. 29, pp. 26–33, 2016.

[100] T. Moroishi, H. W. Park, B. Qin, Q. Chen, Z. Meng, S. W. Plouffe, K. Taniguchi, F. X. Yu, M. Karin, D. Pan, and K. L. Guan, "A yap/taz-induced feedback mechanism regulates hippo pathway homeostasis," *Genes Dev*, vol. 29, no. 12, pp. 1271–84, 2015.

[101] D. J. Williamson, M. A. Fascione, M. E. Webb, and W. B. Turnbull, "Efficient n-terminal labeling of proteins by use of sortase," *Angew Chem Int Ed Engl*, vol. 51, no. 37, pp. 9377–80, 2012.

[102] F. Liu, E. Y. Luo, D. B. Flora, and A. R. Mezo, "Irreversible sortase a-mediated ligation driven by diketopiperazine formation," *J Org Chem*, vol. 79, no. 2, pp. 487–92, 2014.

[103] N. Sato, X. B. Cheng, S. Kohi, A. Koga, and K. Hirata, "Targeting hyaluronan for the treatment of pancreatic ductal adenocarcinoma," *Acta Pharm Sin B*, vol. 6, no. 2, pp. 101–5, 2016.

[104] N. Sato, S. Kohi, K. Hirata, and M. Goggins, "Role of hyaluronan in pancreatic cancer biology and therapy: Once again in the spotlight," *Cancer Sci*, vol. 107, no. 5, pp. 569–75, 2016.
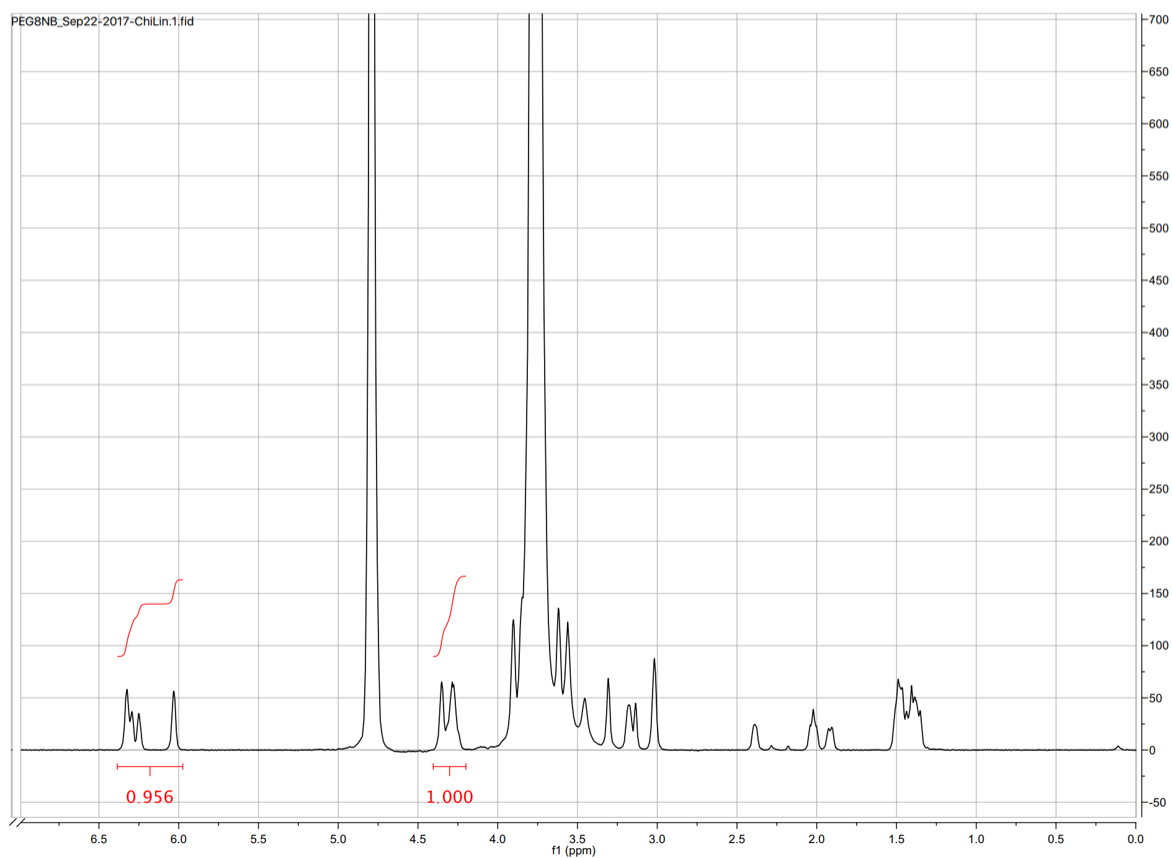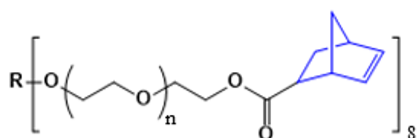
APPENDICES

A. PEG8NB NMR

Fig. A.1. ^{1}H NMR spectrum for PEG8NB (20 kDa). Note that R represents the pentaerythritol core.

B. PCR PRIMERS

Table B.1. Gene Sequences Used for Real time PCR.

Gene	Sequence	Reference
GAPDH	f: GAAGGTGAAGGTCGGAGTC	Ling H, et al.
	r: GAAGATGGTGATGGATTTC	Oncogene 2010;29:4543-54
SHH	f: GGAAGCAGCCTCCCGATT	Jabari S, et al.
	r: CGACTCCAAGGCACATATCCA	Int. J. Oncol. 2009:45;69-80
ANKRD1	f: GCTGGAGCCCAGATTGAA	Songstad NT, et al.
	r: CTCCACGACATGCCCAGT	PLoS One 2014:9:e89559